iScience

CellPress
OPEN ACCESS

Article

Machine learning unveils immune-related signature in multicenter glioma studies

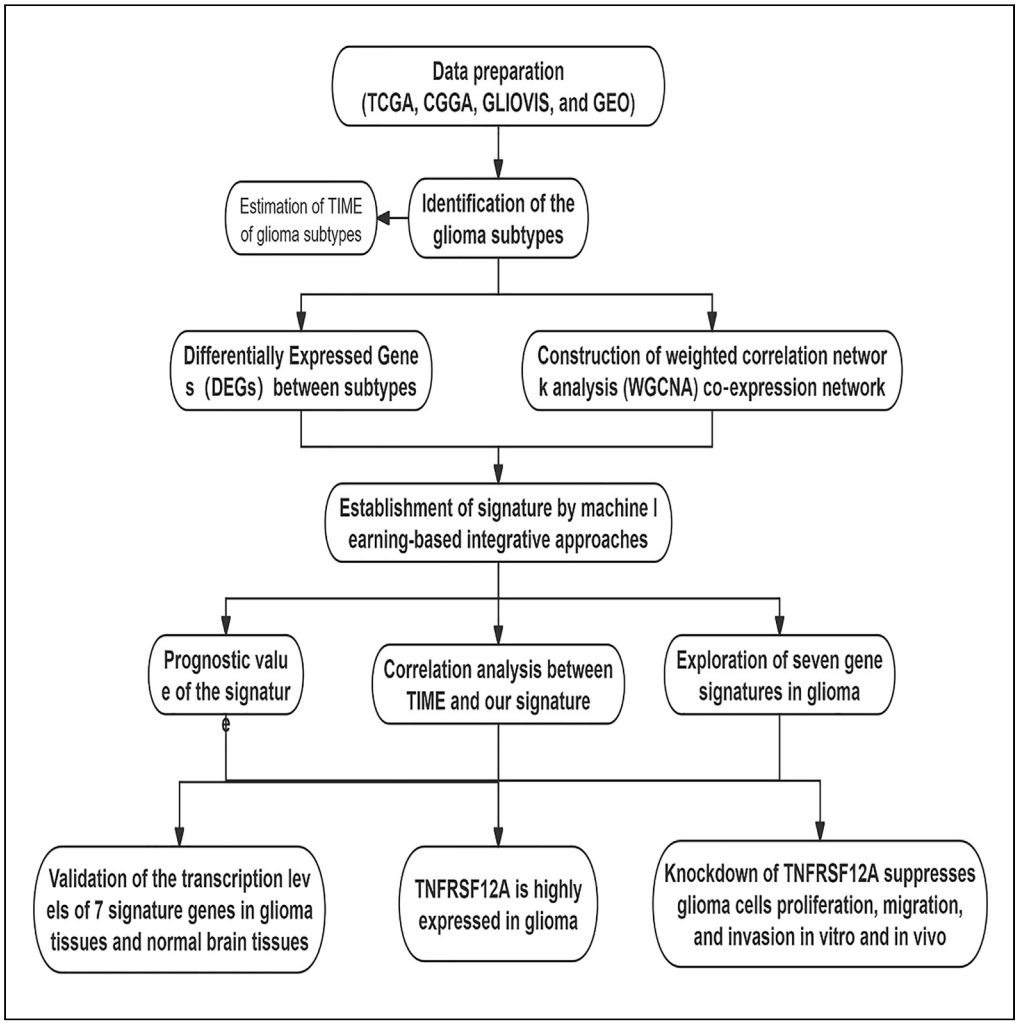

Sha Yang, Xiang Wang, Renzheng Huan, ..., Guoqiang Han, Jiqin Zhang, Ying Tan

hanguoqiang@gz5055.com (G.H.)
zhangjiqin@gz5055.com (J.Z.)
tanying@gz5055.com (Y.T.)

Highlights

Robust ML model stratifies glioma patients, enhancing prognostic precision

CIPS is a prognostic factor and insight into glioma immune microenvironment

CIPS improves outcomes in glioma patients, showing practical implementation in treatments

IGFBP2 and TNFRSF12A pinpointed as tumor markers, paving way for targeted interventions

Yang et al., iScience *27*, 109317
April 19, 2024
https://doi.org/10.1016/j.isci.2024.109317

iScience

CellPress
OPEN ACCESS

Article

Machine learning unveils immune-related signature in multicenter glioma studies

Sha Yang,[1,6] Xiang Wang,[2,6] Renzheng Huan,[3] Mei Deng,[4] Zhuo Kong,[4] Yunbiao Xiong,[4] Tao Luo,[4] Zheng Jin,[4] Jian Liu,[1,4] Liangzhao Chu,[2] Guoqiang Han,[4,7,*] Jiqin Zhang,[5,7,*] and Ying Tan[4,7,8,*]

SUMMARY

In glioma molecular subtyping, existing biomarkers are limited, prompting the development of new ones. We present a multicenter study-derived consensus immune-related and prognostic gene signature (CIPS) using an optimal risk score model and 101 algorithms. CIPS, an independent risk factor, showed stable and powerful predictive performance for overall and progression-free survival, surpassing traditional clinical variables. The risk score correlated significantly with the immune microenvironment, indicating potential sensitivity to immunotherapy. High-risk groups exhibited distinct chemotherapy drug sensitivity. Seven signature genes, including IGFBP2 and TNFRSF12A, were validated by qRT-PCR, with higher expression in tumors and prognostic relevance. TNFRSF12A, upregulated in GBM, demonstrated inhibitory effects on glioma cell proliferation, migration, and invasion. CIPS emerges as a robust tool for enhancing individual glioma patient outcomes, while IGFBP2 and TNFRSF12A pose as promising tumor markers and therapeutic targets.

INTRODUCTION

Glioma is highly heterogeneous, and histological differentiation has no effect on the current clinical treatment. However, the diversity of molecular subtypes can better explain the heterogeneity of glioma, which is significantly related to the treatment and prognosis of patients.[1,2] Therefore, the 2021 WHO CNS5 has updated the classification of tumor types by considering the molecular markers of different tumor types and combining with histological characteristics, which will bring more benefits and meaningful guidance to the clinic.[1–7] Resection should be completed as soon as possible even for LGG to avoid malignant progression and accurately identify the molecular subtypes.[8] High-risk LGG has a high probability of recurrence and requires standard postoperative treatment, including radiotherapy and adjuvant chemotherapy.[9] For GBM, standard treatment should include maximum total tumor resection, locoregional radiotherapy, and concurrent temozolomide (TMZ) chemotherapy.[10,11] In addition, immunotherapy have made significant progress in preclinical and clinical trials.[12] However, the majority of gliomas do not fully recover and do not achieve the ideal prognosis, which is largely attributed to the molecular heterogeneity of the tumor microenvironment (TME) of glioma.[13,14] There is therefore an urgent need to identify predictive biomarkers to guide clinical decision making while developing new and more effective targeted therapies.

The TME of glioma is highly heterogeneous, which is involved in the recurrence, metastasis, and drug resistance.[15–17] The interaction between glioma cells and immune cells promotes the process of carcinogenesis. The establishment of glioma stem cells and the involvement of immune cells in TME become important factors in tumor resistance to therapy.[18–20] Based on genetic alterations in the primary tumor, changes in the TME enable tumor cells to evade host tumor surveillance mechanisms and promote highly aggressive tumor growth.[21,22] In addition, these combined effects further affect the molecular heterogeneity of gliomas. The tumor immune microenvironment (TIME) is also determined by the interaction of the respective molecular biological states of the tumor.[22–25] Interestingly, a systemic immunodeficiency has been found in glioma patients,[26] while glioma can induce an immune response.[27,28] The prognosis of gliomas has been associated with the presence of immune cells in the TME.[29,30] However, the exact interplay between the molecular biological characteristics of cells and the TIME has not been elucidated. A detailed description of these complex mechanisms is essential for tuning and developing therapeutic strategies that may overcome immune escape in gliomas. On the one hand, effective immunotherapy can be selected based on individual molecular status, and on the other hand, the molecular status can be changed by targeted therapy.

[1]Guizhou University Medical College, Guiyang 550025, Guizhou Province, China
[2]Department of Neurosurgery, the Affiliated Hospital of Guizhou Medical University, Guiyang 550004, China
[3]Department of Neurosurgery, The Second Affiliated Hospital of Chongqing Medical University, Chongqing 400010, China
[4]Department of Neurosurgery, Guizhou Provincial People's Hospital, Guiyang, China
[5]Department of Anesthesiology, Guizhou Provincial People's Hospital, Guiyang, China
[6]These authors contributed equally
[7]These authors contributed equally
[8]Lead contact
*Correspondence: hanguoqiang@gz5055.com (G.H.), zhangjiqin@gz5055.com (J.Z.), tanying@gz5055.com (Y.T.)
https://doi.org/10.1016/j.isci.2024.109317

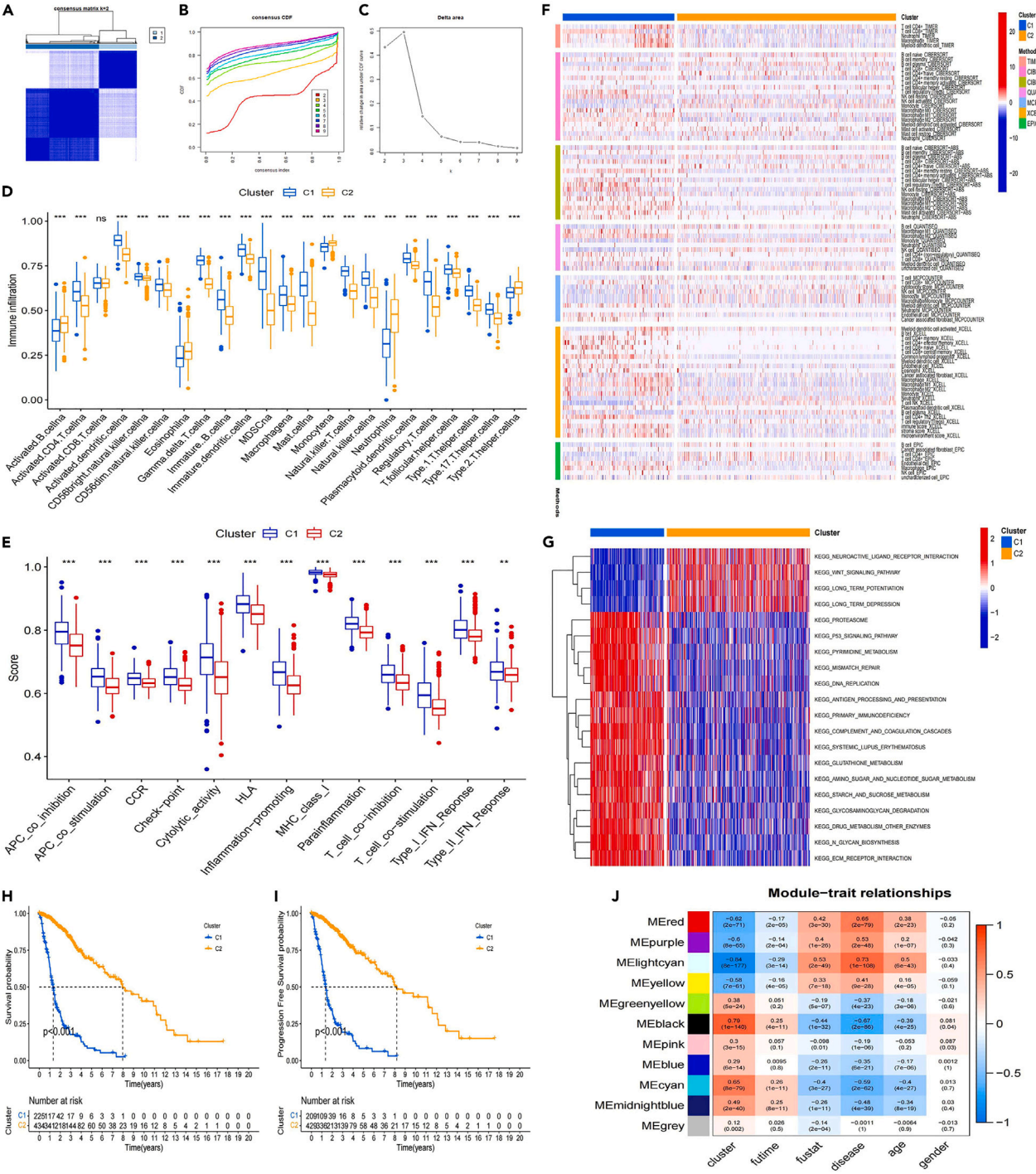

Figure 1. Identification of immune-related genes

(A) The consensus score matrix of all samples when k = 2, showing the clustering stability after the 1000 times k-means cluster approach.

(B) The CDF curves of consensus matrix for each k.

(C) The relative change in area under CDF curve of consensus matrix for each k.

(D) The results of single-sample gene set enrichment analysis (ssGSEA): the immune infiltration for each cluster.

(E) The results of ssGSEA: the immune function for each cluster.

Figure 1. *Continued*

(F) The results of seven other algorithms, including TIMER, CIBERSORT, CIBERSORT−ABS, QUANTISEQ, MCPCOUNTER, XCELL, and EPIC: the immune infiltration for each cluster.

(G) The heatmap showed the results of GSVA analysis for each cluster.

(H and I) Kaplan-Meier OS (H) and RFS (I) curves comparing the patients in different cluster.

(J) Heatmap of the correlation between module eigengenes and clinical traits. Data are represented as mean ± SEM.

Machine learning has emerged as a transformative tool in medical research, significantly enhancing diagnostic and prognostic capabilities in various complex diseases. Its applications range from predicting protein crystallization processes and assessing drug-food interactions to evaluating cancer prognosis in types such as triple-negative breast cancer and lung adenocarcinoma.[31–34] Notably, machine learning has been instrumental in delineating tumor-infiltrating immune cell signatures in gliomas, offering deeper insights into the interactions within the TME.[35,36] These advancements demonstrate the versatility and efficacy of machine learning methods in addressing the intricacies of complex diseases like glioma.

According to glioma CNS5 grading, tumor mutational burden (TMB), tumor infiltrating lymphocytes (TIL), and microsatellite instability (MSI) can predict the prognosis and response to immunotherapy.[37–39] However, it only applies to a limited number of glioma patients. Therefore, further consideration of molecular biological characteristics also needed. In this study, we attempted to develop and validate a risk stratification signature in glioma patients by combining bioinformatics and machine learning algorithms to screen relevant molecular signatures to evaluate the prognosis, recurrence, and treatment benefit of glioma. The correlation between risk stratification signature and TIME was also explored. Finally, we validated our findings by *in vitro and in vivo* experiments. The aim of this study is to optimize precision treatment, improve new ideas for targeted therapy, and further improve the clinical outcome of patients.

RESULTS

Construction of consensus clusters

PCA plots show no batch effect on processed data.(Figure S1) Firstly, 788 DEGs between glioma and normal brain samples were found in training cohort, and then the expression profiles of 788 genes was applied to find 2 clusters by consensus clustering algorithm.(Figures 1A–1C, and Table S1) Next, ssGSEA was performed to evaluate the 28 immune cells infiltration in each cluster. The results show that cluster 1 having a markedly higher overall infiltration abundance of all immune cells compare to cluster 2. (Figure 1D and S2) Similarly, the immune function activation of C1 cluster was more obvious. (Figure 1E) Therefore, we speculated that C1 was more likely to be "immune-hot" tumors and C2 was more likely to be "immune-cold" tumors. To ensure that the evaluation of immune cells in the two consensus clusters was more accurate, we also used the other seven algorithms. The heatmap showed that the results of the other seven algorithms were consistent with those of ssGSEA. (Figure 1F) Further GSVA analysis found that Cluster 1 enriched various pathways related to immunity and metabolism, such as antigen processing and presentation, complement and coagulation cascades, glutathione metabolism, amino sugar, and nucleotide sugar metabolism. (Figure 1G) Kaplan–Meier curves of OS and PFS showed that glioma patients in cluster 2 have a better prognosis.(Figures 1H and 1I) In addition, DEGs between cluster 1 and cluster 2 were identified for further analyze. GO analysis revealed that these DEGs were significantly involved in immune related pathway, such as leukocyte/lymphocyte mediated immunity, adaptive immune response, humoral immune response.(Figure S3A) KEGG pathway enrichment analysis also indicated the roles of these DEGs in Natural killer cell mediated cytotoxicity, Th1 and Th2 cell differentiation, and so on. (Figure S3B) Similarly, cluster 1 was found to have high expression of a gene set related to naive CD8 T cell in GSEA (Figures S3C and S3D).

Identification of molecular subtypes-related module and intersecting DEGs

A co-expression network was constructed by the weighted correlation network analysis (WGCNA) with the soft threshold $\beta = 11$ (no scale R2 = 0.916). (Figure S4) Then, 11 modules were identified and module-trait relationships were shown in Figure 1J. The correlations between each module and each feature, such as clusters, survival time, survival state, WHO stage, age, and gender were calculated. The strongest negative correlation was observed between lightcyan module and cluster. Subsequently, we identified the intersection genes of DEGs between two clusters and module genes in lightcyan module. Then, univariate cox regression analysis was performed to identify potential prognostic genes from these intersection genes. ($p < 0.05$) Finally, 41 gene was considered potential prognostic genes for further analysis.(Table S2).

Construction of a prognostic consensus signature

These 41 potential prognostic genes were subjected to our machine learning-based integrative procedure to develop a consensus immune-related and prognostic-related gene signature (CIPS). In the training cohort, a few algorithms displayed extreme accuracy, such as RSF, StepCox[backward/both]+RSF, and CoxBoost+RSF, with its C-index even over 0.95. In all cohort, the models, including RSF and Lasso+RSF, with the highest average Cindex (0.754) was considered the optimal model. Considering that fewer signature are finally determined in the Lasso+RSF model, we finally determined this model as the optimal one.(Figure 2A) Therefore, 7 signature genes in Lasso+RSF model were used to weight risk score for each patient by coefficients of those genes.(Figure 2B) Subsequently, all glioma patients were divided into high-risk and low-risk subgroups based on the median risk score in the training cohort. Kaplan-Meier analysis revealed that significant differences between high-risk and low-risk subgroups both in training and verification cohorts ($p < 0.001$), and low-risk subgroup was associated with a better OS.(Figures 2C and 2D) Moreover, patients in low-risk subgroup had a better PFS were determined in all cohort. (Figure 2E) In order to further

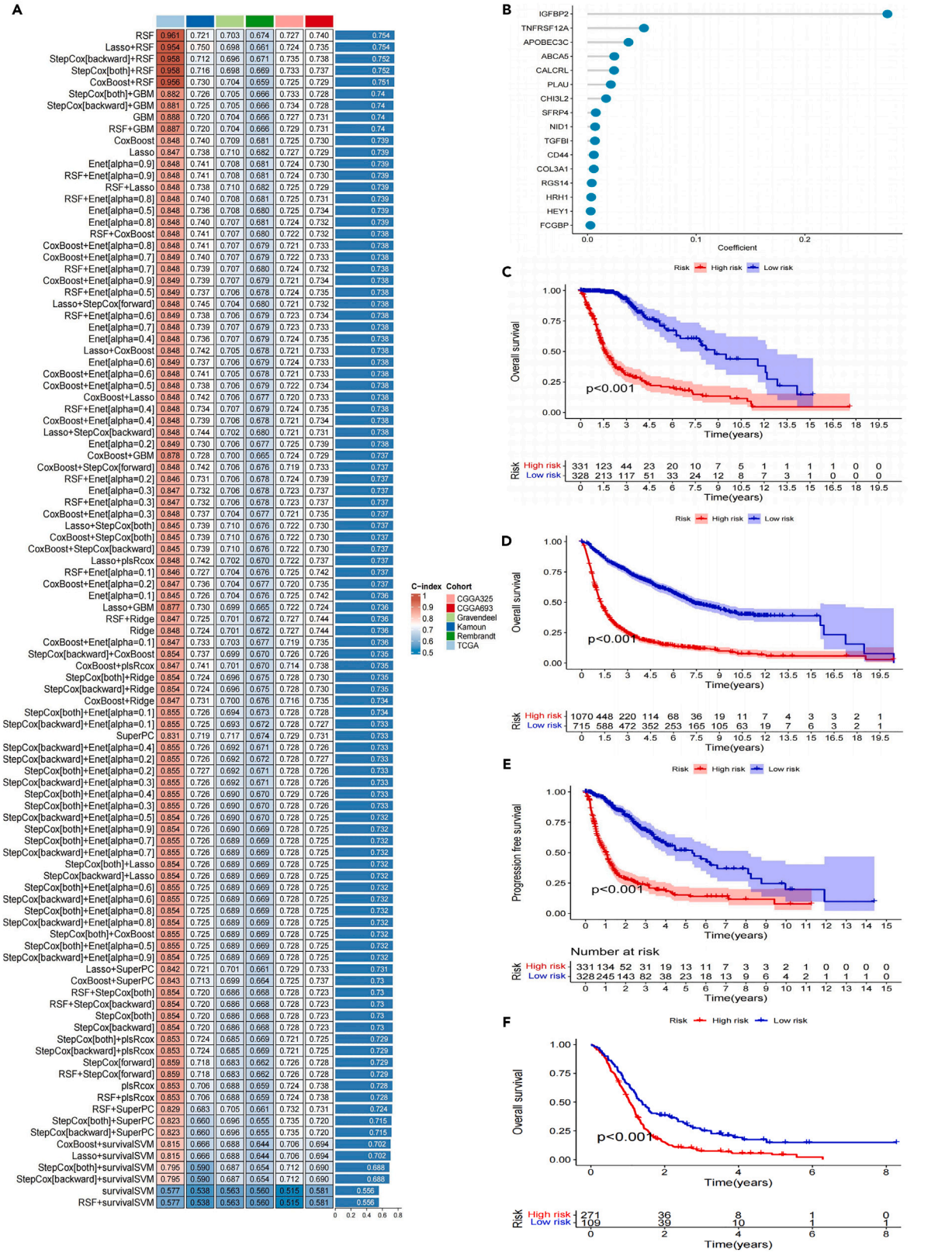
A
RSF 0.961 0.721 0.703 0.674 0.727 0.740 0.754
Lasso+RSF 0.954 0.750 0.698 0.661 0.724 0.735 0.754
StepCox[backward]+RSF 0.958 0.712 0.696 0.671 0.735 0.738 0.752
StepCox[both]+RSF 0.958 0.716 0.698 0.669 0.733 0.737 0.752
CoxBoost+RSF 0.956 0.730 0.704 0.659 0.725 0.729 0.751
StepCox[both]+GBM 0.882 0.726 0.705 0.666 0.733 0.728 0.74
StepCox[backward]+GBM 0.881 0.725 0.705 0.666 0.734 0.728 0.74
GBM 0.888 0.720 0.704 0.666 0.727 0.731 0.74
RSF+GBM 0.887 0.720 0.704 0.666 0.729 0.731 0.74
CoxBoost 0.848 0.740 0.709 0.681 0.725 0.730 0.739
Lasso 0.847 0.738 0.710 0.682 0.727 0.729 0.739
Enet[alpha=0.9] 0.848 0.741 0.708 0.681 0.724 0.730 0.739
RSF+Enet[alpha=0.9] 0.848 0.741 0.708 0.681 0.724 0.730 0.739
RSF+Lasso 0.848 0.738 0.710 0.682 0.725 0.729 0.739
RSF+Enet[alpha=0.8] 0.848 0.740 0.708 0.681 0.725 0.731 0.739
Enet[alpha=0.5] 0.848 0.736 0.708 0.680 0.725 0.734 0.739
Enet[alpha=0.8] 0.848 0.740 0.707 0.681 0.724 0.732 0.739
RSF+CoxBoost 0.848 0.741 0.707 0.680 0.722 0.732 0.738
CoxBoost+Enet[alpha=0.8] 0.848 0.741 0.707 0.679 0.721 0.733 0.738
CoxBoost+Enet[alpha=0.7] 0.849 0.740 0.707 0.679 0.722 0.733 0.738
RSF+Enet[alpha=0.7] 0.848 0.739 0.707 0.680 0.724 0.732 0.738
CoxBoost+Enet[alpha=0.9] 0.849 0.739 0.707 0.679 0.721 0.734 0.738
RSF+Enet[alpha=0.5] 0.849 0.737 0.706 0.678 0.724 0.735 0.738
Lasso+StepCox[forward] 0.848 0.745 0.704 0.680 0.721 0.732 0.738
RSF+Enet[alpha=0.6] 0.849 0.738 0.706 0.679 0.723 0.734 0.738
Enet[alpha=0.7] 0.848 0.739 0.707 0.679 0.723 0.733 0.738
Enet[alpha=0.4] 0.848 0.736 0.707 0.679 0.724 0.735 0.738
Lasso+CoxBoost 0.848 0.742 0.705 0.678 0.721 0.733 0.738
Enet[alpha=0.6] 0.849 0.737 0.706 0.679 0.724 0.733 0.738
CoxBoost+Enet[alpha=0.6] 0.848 0.741 0.705 0.678 0.721 0.733 0.738
CoxBoost+Enet[alpha=0.5] 0.848 0.738 0.706 0.679 0.722 0.734 0.738
CoxBoost+Lasso 0.848 0.742 0.706 0.677 0.720 0.733 0.738
RSF+Enet[alpha=0.4] 0.848 0.734 0.707 0.679 0.724 0.735 0.738
CoxBoost+Enet[alpha=0.4] 0.848 0.739 0.706 0.678 0.721 0.734 0.738
Lasso+StepCox[backward] 0.848 0.744 0.702 0.680 0.721 0.731 0.738
Enet[alpha=0.2] 0.849 0.730 0.706 0.677 0.725 0.739 0.738
CoxBoost+GBM 0.878 0.728 0.700 0.665 0.724 0.729 0.737
CoxBoost+StepCox[forward] 0.848 0.742 0.706 0.676 0.719 0.733 0.737
RSF+Enet[alpha=0.2] 0.846 0.731 0.706 0.678 0.724 0.739 0.737
Enet[alpha=0.3] 0.847 0.732 0.706 0.678 0.723 0.737 0.737
RSF+Enet[alpha=0.3] 0.847 0.732 0.706 0.678 0.723 0.737 0.737
CoxBoost+Enet[alpha=0.3] 0.848 0.737 0.704 0.677 0.721 0.735 0.737
Lasso+StepCox[both] 0.845 0.739 0.710 0.676 0.722 0.730 0.737
CoxBoost+StepCox[both] 0.845 0.739 0.710 0.676 0.722 0.730 0.737
CoxBoost+StepCox[backward] 0.845 0.739 0.710 0.676 0.722 0.730 0.737
Lasso+plsRcox 0.848 0.742 0.702 0.670 0.722 0.737 0.737
RSF+Enet[alpha=0.1] 0.846 0.727 0.704 0.676 0.725 0.742 0.737
CoxBoost+Enet[alpha=0.2] 0.847 0.736 0.704 0.677 0.720 0.735 0.737
Enet[alpha=0.1] 0.845 0.726 0.704 0.676 0.725 0.742 0.736
Lasso+GBM 0.877 0.730 0.699 0.665 0.722 0.724 0.736
RSF+Ridge 0.847 0.725 0.701 0.672 0.727 0.744 0.736
Ridge 0.848 0.724 0.701 0.672 0.727 0.744 0.736
CoxBoost+Enet[alpha=0.1] 0.847 0.733 0.703 0.677 0.719 0.735 0.736
StepCox[backward]+CoxBoost 0.854 0.737 0.699 0.670 0.726 0.726 0.735
CoxBoost+plsRcox 0.847 0.741 0.701 0.670 0.714 0.738 0.735
StepCox[both]+Ridge 0.854 0.724 0.696 0.675 0.728 0.730 0.735
StepCox[backward]+Ridge 0.854 0.724 0.696 0.675 0.728 0.730 0.735
CoxBoost+Ridge 0.847 0.731 0.700 0.676 0.716 0.735 0.734
StepCox[both]+Enet[alpha=0.1] 0.855 0.726 0.694 0.673 0.728 0.728 0.734
StepCox[backward]+Enet[alpha=0.1] 0.855 0.725 0.693 0.672 0.728 0.727 0.733
SuperPC 0.831 0.719 0.717 0.674 0.729 0.731 0.733
StepCox[backward]+Enet[alpha=0.4] 0.855 0.726 0.692 0.671 0.728 0.726 0.733
StepCox[backward]+Enet[alpha=0.2] 0.855 0.726 0.692 0.672 0.728 0.727 0.733
StepCox[both]+Enet[alpha=0.2] 0.855 0.727 0.692 0.671 0.728 0.726 0.733
StepCox[backward]+Enet[alpha=0.3] 0.855 0.726 0.692 0.671 0.728 0.726 0.733
StepCox[both]+Enet[alpha=0.4] 0.855 0.726 0.690 0.670 0.729 0.726 0.733
StepCox[both]+Enet[alpha=0.3] 0.855 0.726 0.690 0.670 0.728 0.726 0.733
StepCox[backward]+Enet[alpha=0.5] 0.854 0.726 0.690 0.670 0.728 0.725 0.732
StepCox[both]+Enet[alpha=0.9] 0.854 0.726 0.690 0.669 0.728 0.725 0.732
StepCox[both]+Enet[alpha=0.7] 0.855 0.726 0.689 0.669 0.728 0.725 0.732
StepCox[backward]+Enet[alpha=0.7] 0.855 0.726 0.689 0.669 0.728 0.725 0.732
StepCox[both]+Lasso 0.854 0.726 0.689 0.669 0.728 0.725 0.732
StepCox[backward]+Lasso 0.854 0.726 0.689 0.669 0.728 0.725 0.732
StepCox[both]+Enet[alpha=0.6] 0.855 0.725 0.689 0.669 0.728 0.725 0.732
StepCox[backward]+Enet[alpha=0.6] 0.855 0.725 0.689 0.669 0.728 0.725 0.732
StepCox[both]+Enet[alpha=0.8] 0.854 0.725 0.689 0.669 0.728 0.725 0.732
StepCox[backward]+Enet[alpha=0.8] 0.854 0.725 0.689 0.669 0.728 0.725 0.732
StepCox[both]+CoxBoost 0.855 0.725 0.689 0.669 0.728 0.725 0.732
StepCox[both]+Enet[alpha=0.5] 0.855 0.725 0.689 0.669 0.728 0.725 0.732
StepCox[backward]+Enet[alpha=0.9] 0.854 0.725 0.689 0.669 0.728 0.725 0.732
Lasso+SuperPC 0.842 0.721 0.701 0.661 0.729 0.733 0.731
CoxBoost+SuperPC 0.843 0.713 0.699 0.664 0.725 0.737 0.73
RSF+StepCox[both] 0.854 0.720 0.686 0.668 0.728 0.723 0.73
RSF+StepCox[backward] 0.854 0.720 0.686 0.668 0.728 0.723 0.73
StepCox[both] 0.854 0.720 0.686 0.668 0.728 0.723 0.73
StepCox[backward] 0.854 0.720 0.686 0.668 0.728 0.723 0.73
StepCox[both]+plsRcox 0.853 0.724 0.685 0.669 0.721 0.725 0.729
StepCox[backward]+plsRcox 0.853 0.724 0.685 0.669 0.721 0.725 0.729
StepCox[forward] 0.859 0.718 0.683 0.662 0.726 0.728 0.729
RSF+StepCox[forward] 0.859 0.718 0.683 0.662 0.726 0.728 0.729
plsRcox 0.853 0.706 0.688 0.659 0.724 0.738 0.728
RSF+plsRcox 0.853 0.706 0.688 0.659 0.724 0.738 0.728
RSF+SuperPC 0.829 0.683 0.705 0.661 0.732 0.731 0.724
StepCox[both]+SuperPC 0.823 0.660 0.696 0.655 0.735 0.720 0.715
StepCox[backward]+SuperPC 0.823 0.660 0.696 0.655 0.735 0.720 0.715
CoxBoost+survivalSVM 0.815 0.666 0.688 0.644 0.706 0.694 0.702
Lasso+survivalSVM 0.815 0.666 0.688 0.644 0.706 0.694 0.702
StepCox[both]+survivalSVM 0.795 0.590 0.687 0.654 0.712 0.690 0.688
StepCox[backward]+survivalSVM 0.795 0.590 0.687 0.654 0.712 0.690 0.688
survivalSVM 0.577 0.538 0.563 0.560 0.515 0.581 0.556
RSF+survivalSVM 0.577 0.538 0.563 0.560 0.515 0.581 0.556
0 0.2 0.4 0.6 0.8
C-index
1 0.9 0.8 0.7 0.6 0.5
Cohort
CGGA325
CGGA693
Gravendeel
Kamoun
Rembrandt
TCGA
B
IGFBP2
TNFRSF12A
APOBEC3C
ABCA5
CALCRL
PLAU
CHI3L2
SFRP4
NID1
TGFBI
CD44
COL3A1
RGS14
HRH1
HEY1
FCGBP
0.0 0.1 0.2
Coefficient
C
Risk High risk Low risk
Overall survival
p<0.001
Time(years)
Risk
High risk 331 123 44 23 20 10 7 5 1 1 1 1 0 0
Low risk 328 213 117 51 33 24 12 8 7 3 1 0 0 0
D
Risk High risk Low risk
Overall survival
p<0.001
Time(years)
Risk
High risk 1070 448 220 114 68 36 19 11 7 4 3 3 2 1
Low risk 715 588 472 352 253 165 105 63 19 7 6 3 2 1
E
Risk High risk Low risk
Progression free survival
p<0.001
Time(years)
Number at risk
Risk
High risk 331 134 52 31 19 13 11 7 3 3 2 1 0 0 0 0
Low risk 328 245 143 82 38 23 18 13 9 6 4 2 1 1 1 0
F
Risk High risk Low risk
Overall survival
p<0.001
Time(years)
Risk
High risk 271 36 8 1 0
Low risk 109 39 10 1 1

Figure 2. Construction and validation of CIPS model

(A) C-indices of 101 kinds of prediction models across all validation datasets.

(B) Coefficients of 7 genes finally obtained in RSF.

(C and D) OS analysis of risk score according to the CIPS in TCGA-GBMLGG (C) and verification cohorts (D; glioma cohorts from CGGA and GLIOVIS) based on the Kaplan-Meier plotter.

(E) PFS analysis of risk score according to the CIPS in TCGA-GBMLGG based on the Kaplan-Meier plotter.

(F) OS analysis of risk score according to the CIPS in 6 GEO cohorts (GSE7696, GSE42670, GSE43378, GSE50021, GSE72951, and GSE83300) based on the Kaplan-Meier plotter.

verify the accuracy of our risk score model, we divided the samples containing 6 GEO cohorts into high and low risk groups, and the KM curve showed that the results were consistent with the previous results, and the prognosis of the high-risk group was worse.(Figure 2F, $p < 0.001$).

Evaluation of the independent prognostic value of CIPS model

Univariate cox regression (HR: 3.30 95% CI (2.86–3.81)) and multivariate cox regression (HR: 2.503 95% CI (2.041–3.069)) analysis showed that risk-score was an independent prognostic factor for glioma patients. (Figures 3A and 3B) Thus, a nomogram was established to estimate 1-, 3-, and 5-year OS for glioma patients, which incorporated clinical parameters and risk score. (Figure 3C) Furthermore, the AUC value of risk score was calculated for predicting OS at 1-, 3-, and 5-year, and the AUC was 0.880, 0.911 and 0.828, respectively. (Figure 3D) Then, we also calculated the AUC of other clinical factors for predicting OS at 5-year, and found that AUC of risk score was larger, indicating the better the prediction effect of our model. (Figure 3E) The 1-, 3-, 5-year calibration curves proved good predictive effect of the nomogram model.(Figure 3F) At the same time, the DCA curve shows that nomograms can better predict 1-year, 3-year, and 5-year OS.(Figures S5A–S5C) Compared to the C-index and restricted mean survival (RMS) of four published risk models,[40–43] the risk model we developed has great advantages.(Figures S5D and S5E).

We also compared differences in risk scores across clinical subgroups, and found that patients with GBM or patients older than 65 years had significant higher risk score than those with LGG or younger than 65 years, respectively ($p < 0.001$, Figures 3G and 3H). In addition, the result showed that significant differences in risk scores among immune subtypes, patients in lymphocyte exhaustion (C4) had significant higher risk score than C3 and C5, and immune calm (C5), mainly low grade gliomas, had significant lower risk score than C3 and C4. (Figure 3I).

Association between TME and risk score

In order to evaluate the correlation between immune cells in TME and risk score, eight algorithms were utilized to evaluate Infiltrating immune cells. The results of ssGSEA showed that the high-risk subgroup had significantly more infiltrating immune cells and significantly activated immune-related functions. (Figures 4A and 4B) The heatmap showed that the infiltrating immune cells in the TME were different between the high- and low-risk subgroups. (Figure 4C) The GSVA results suggested that the pathways related to tumor development, metastasis and drug resistance were active in the high-risk subgroup, such as P53 signaling pathway, cell cycle, JAK STAT signaling pathway. (Figure 4D).

Association between immunotherapy and risk score

The somatic mutation profile of genes as different between two risk subgroups. A total of 399 samples in high-risk subgroup experienced mutations, with a frequency of 91.41%, while 314 samples in low-risk subgroup experienced mutations, with a frequency of 96.91%, as shown in Figure 5A. The stemness index was significantly negatively correlated with the risk score, and stemness index of low-risk subgroup was significantly higher than those of high-risk subgroup. (Figures 5B and 5C) The TMB was significantly positively correlated with the risk score, and TMB of high-risk subgroup was significantly higher than those of low-risk subgroup.(Figures 5D and 5E) Those results indicated that the patients in high-risk subgroup tended to be more sensitive to immunotherapy. The half-maximal inhibitory concentration (IC50) was calculated to predict the treatment response to different drugs, significant difference was observed between high- and low-risk subgroups.(Figure S6) We also investigated the levels of expression of immune checkpoint in training cohort, and the expression of checkpoint genes had an absolute advantage in samples of high-risk subgroup. The TIDE score was significant negatively correlated with the risk score ($R = -0.5, p < 0.001$), TIDE score of high-risk subgroup was significantly lower than those of low-risk subgroup, indicating that patients with high risk score may likely to benefit from immune checkpoint inhibitors (ICI) therapy. (Figures 5F and 5G).

Exploration of seven gene signatures in glioma

Survival analysis showed that there were significant differences in OS and DFS between the two groups when they were grouped by the median expression of seven gene signatures. (Figure S7) CorHeatmap exhibited the correlation between seven genes and infiltrating immune cells. (Figure 6A) In addition, ROC curve showed that these 7 genes could better distinguish normal brain samples from glioma samples (all AUC >0.75), and also better distinguish between high and low risk groups (all AUC >0.6). (Figures 6B–6E and S8) Subsequently, we evaluated the ability of these genes to predict the 1-, 3-, and 5-year OS of glioma patients. The ROC curve showed that IGFBP2 had the strongest prognostic prediction ability, followed by TNFRSF12A and APOBEC3C. (Figures 6F–6H).

Prognostic and immune analysis of IGFBP2 and TNFRSF12A in pan-cancer

We then performed a pan-cancer analysis of IGFBP2 and TNFRSF12A. The results from the TIMER database showed that IGFBP2 and TNFRSF12A expression was significantly higher in most cancer type.(Figures 7A and 8A) The results from the SangerBox website showed

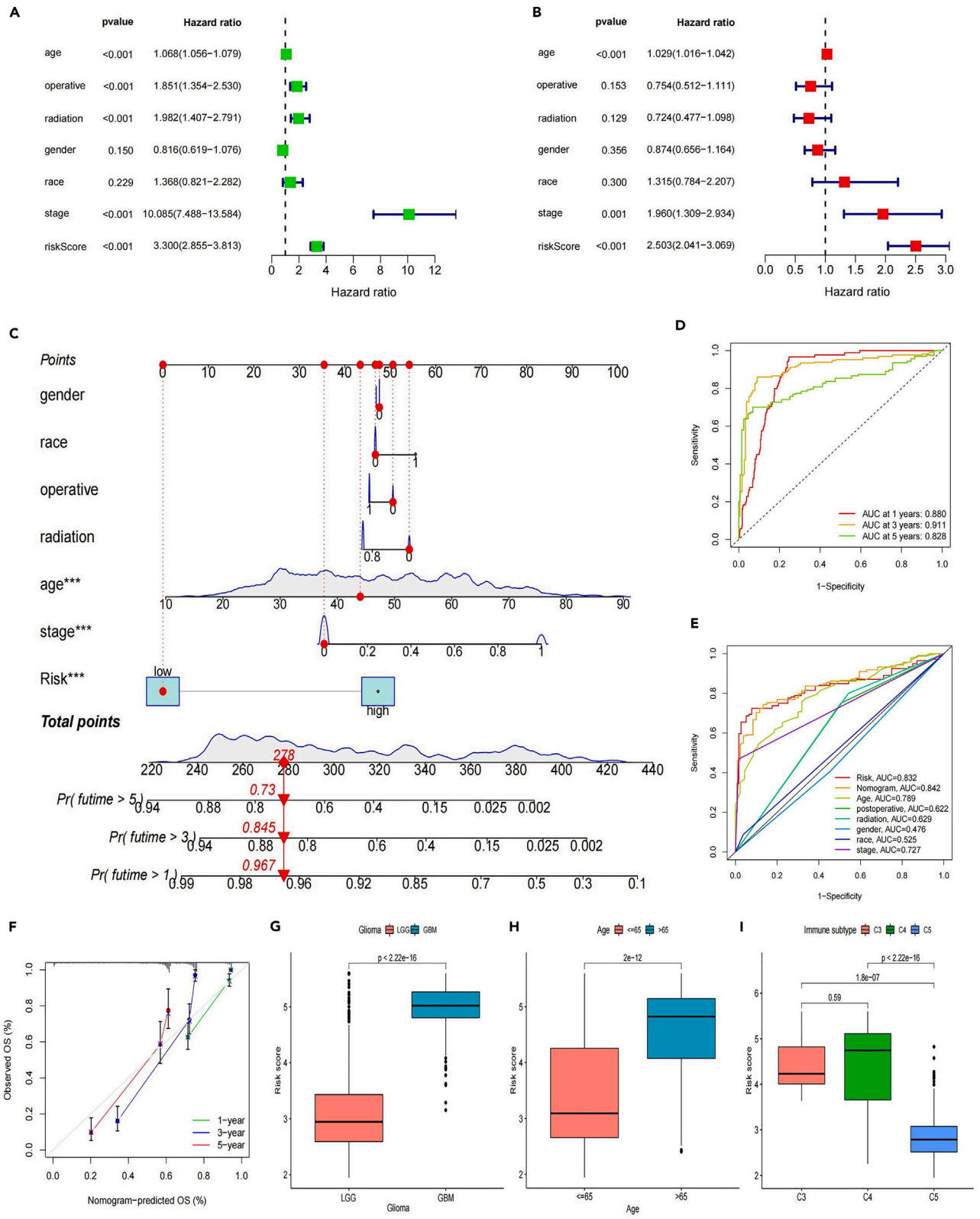

Figure 3. Construction and validation of a nomogram

(A and B) Forest of univariate (A) and multivariate (B) COX regression analyses for OS of glioma patients in the training cohort.

(C) Establishment of OS nomograms for glioma patients.

Figure 3. *Continued*

(D) ROC curves assessing the discriminating ability of the risk score in predicting 1-, 3- and 5-year OS.

(E) ROC curves assessing the discriminating ability of each features in predicting 1-year OS.

(F) 1-, 3- and 5-year calibration plots of OS nomogram model.

(G–I) The bar graph shows the risk scores in different groups, including (G) GBM and LGG, (H) ≤65 years and >65 years, (I) immune subtypes, were significantly different.

that IGFBP2 was significantly upregulated in 20 tumor, and downregulated in 10 tumors, while IGFBP2 was significantly upregulated in 27 tumor, and downregulated in 6 tumors. (Figures 7B and 8B) Subsequently, among ICP genes, strong relationships with IGFBP2 and TNFRSF12A expression and were found in many types of cancer, such as GBMLGG, LGG, Kidney Chromophobe (KICH), and Uveal Melanoma

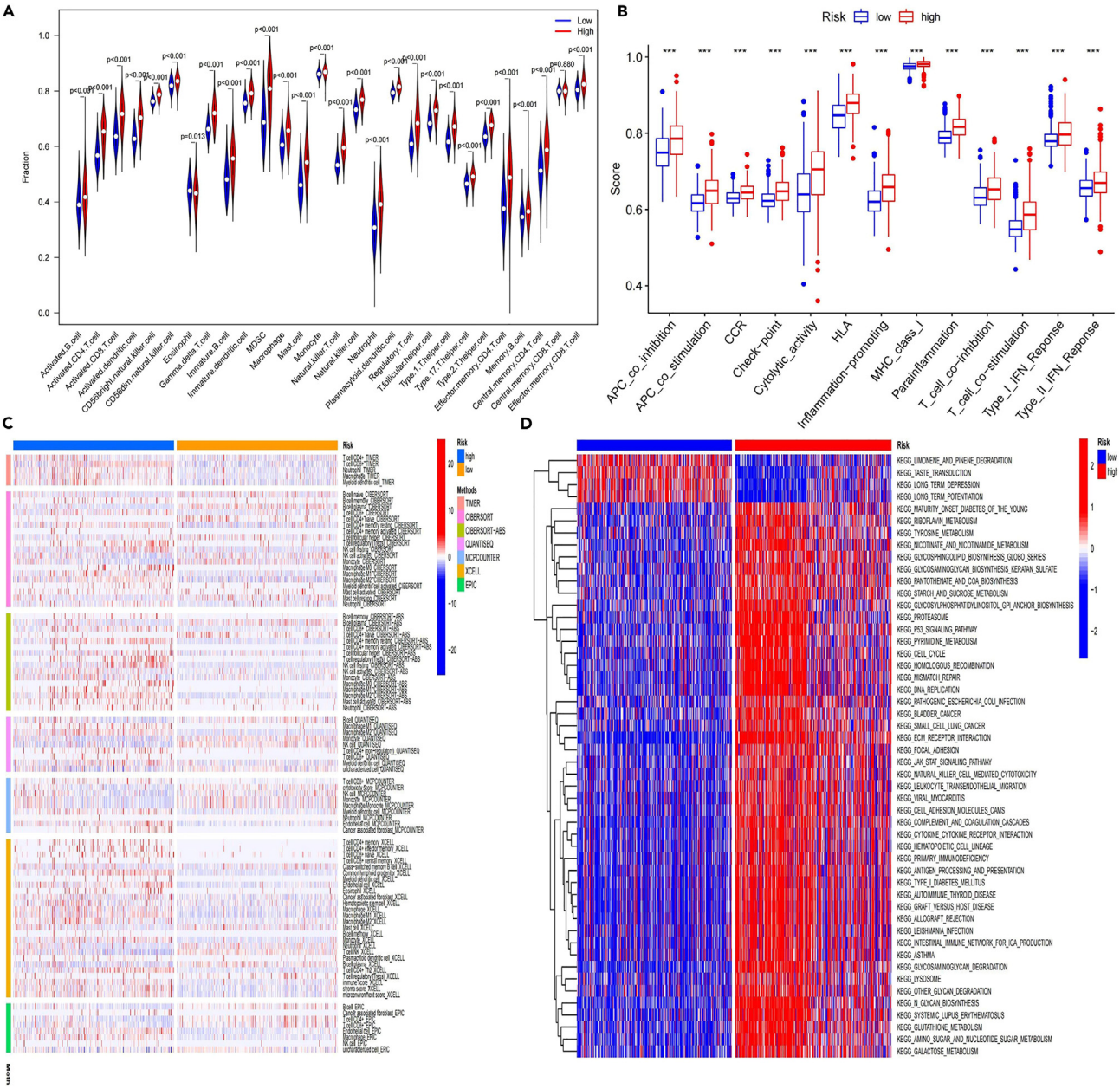

Figure 4. Correlation between TME and risk score

(A) ssGSEA algorithm was used to analyze the proportion of 28 immune cells in high- and low-risk groups.

(B) ssGSEA algorithm was used to analyze the immune-related functions in high- and low-risk groups.

(C) The results of seven other algorithms, including TIMER, CIBERSORT, CIBERSORT−ABS, QUANTISEQ, MCPCOUNTER, XCELL, and EPIC: the immune infiltration in high- and low-risk groups.

(D) Heatmap illustrating the result of GSVA. Data are represented as mean ± SEM.

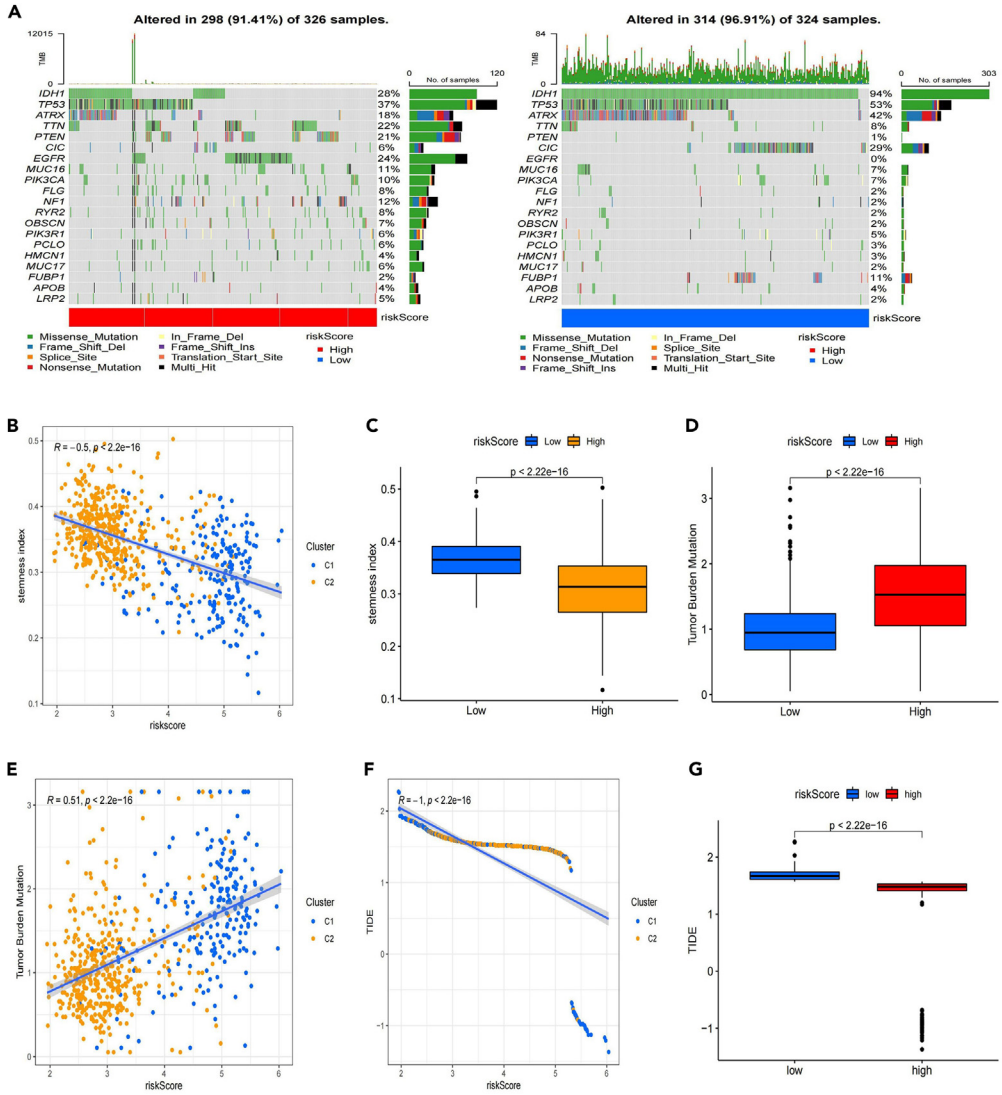

Figure 5. Genomic mutation analysis and Immune status for CIPS signature

(A) Gene mutation frequency in high- and low-risk groups.

(B) The risk score was significantly negatively correlated with the stemness index.

(C and D) Glioma patients with high risk score had lower levels of stemness index (C), and higher TMB (D).

(E and F) The risk score was significantly negatively correlated with (E) TMB, and positive correlated with (F) TIDE.

(G) Glioma patients with high risk score had lower levels of TIDE.

(UVM), indicating the potential of the two genes in immunotherapy. (Figures 7C and 8C) The associations between IGFBP2 and TNFRSF12A expression and DNAss was showed that there were strong positive correlations with IGFBP2 and TNFRSF12A expression in GBMLGG, LGG, Head and Neck squamous cell carcinoma (HNSC), and Lung squamous cell carcinoma (LUSC). (Figures 7D and 8D) The associations between IGFBP2 and TNFRSF12A expression and ESTIMATE was showed in Figures S9 and S10. The results indicated that there were strong positive correlations with IGFBP2 expression in GBMLGG, LGG, UVM, and KICH. Moreover, The xCELL results showed that IGFBP2 was significantly correlated with immune cell infiltration in 44 cancer types, while TNFRSF12A was significantly correlated with immune cell infiltration in 39 cancer types. (Figures 7E and 8E) The above results proved that IGFBP2 and TNFRSF12A play important roles in multiple tumor types, and may play roles by regulating the immune components, immune cell function and mechanism in TME. In addition, positive correlations between IGFBP2 and TNFRSF12A expression and RNA modification in many cancers were observed. (Figures 7F and 8F) Next, via TISIDB website, we found that IGFBP2 and TNFRSF12A expression were related to different immune subtypes. (Figures S11 and S12) What's more, TNFRSF12A expression were related to different molecular subtypes of GBM and LGG.(Figure S13) After Bonferroni correction, IGFBP2 and TNFRSF12A expression were also significantly correlated with characteristic genes and immune cells in many cancer types. (Figures S14 and S15).

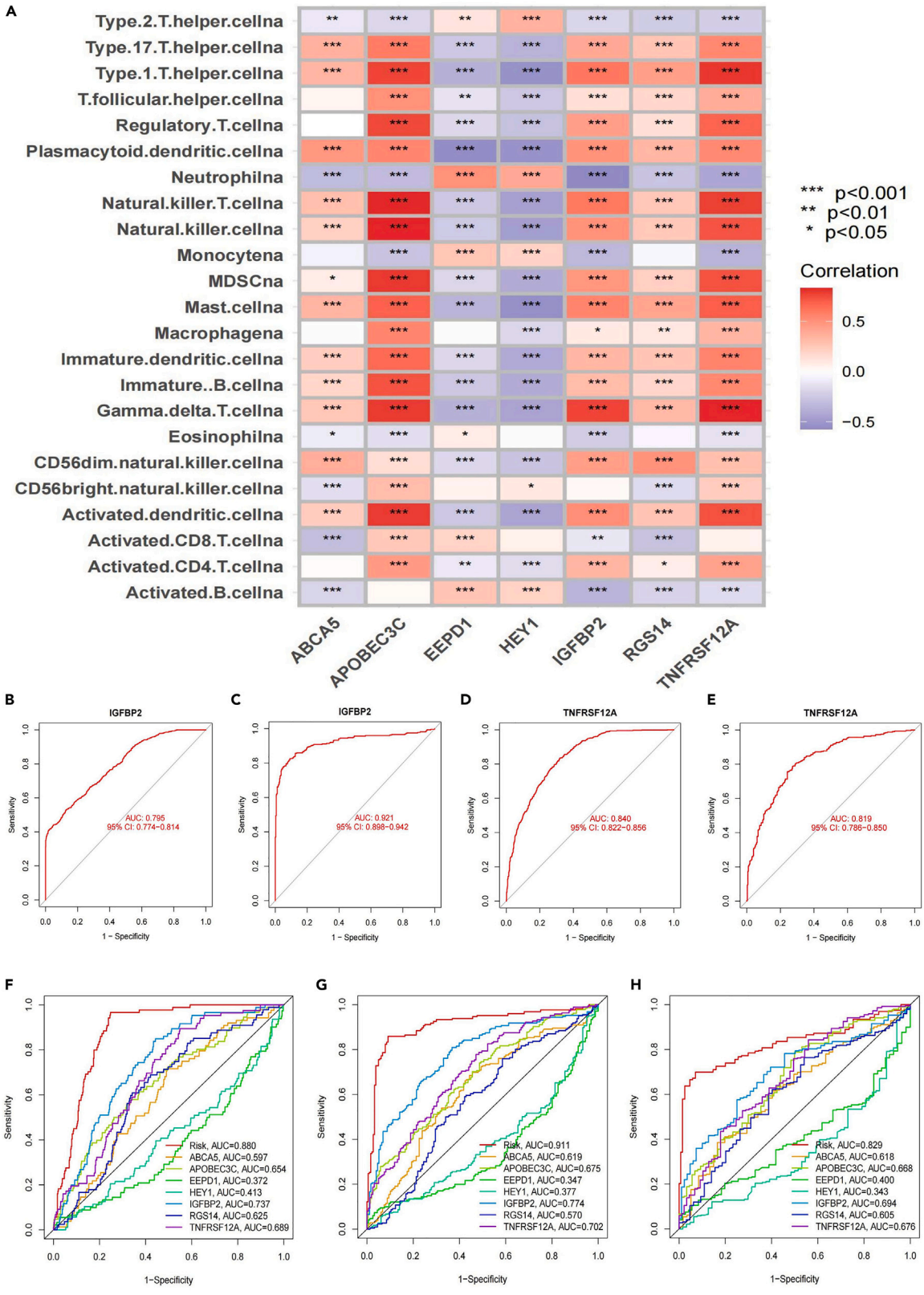
A
Type.2.T.helper.cellna
Type.17.T.helper.cellna
Type.1.T.helper.cellna
T.follicular.helper.cellna
Regulatory.T.cellna
Plasmacytoid.dendritic.cellna
Neutrophilna
Natural.killer.T.cellna
Natural.killer.cellna
Monocytena
MDSCna
Mast.cellna
Macrophagena
Immature.dendritic.cellna
Immature..B.cellna
Gamma.delta.T.cellna
Eosinophilna
CD56dim.natural.killer.cellna
CD56bright.natural.killer.cellna
Activated.dendritic.cellna
Activated.CD8.T.cellna
Activated.CD4.T.cellna
Activated.B.cellna
ABCA5
APOBEC3C
EEPD1
HEY1
IGFBP2
RGS14
TNFRSF12A
*** p<0.001
** p<0.01
* p<0.05
Correlation
0.5
0.0
−0.5
B
IGFBP2
AUC: 0.795
95% CI: 0.774−0.814
C
IGFBP2
AUC: 0.921
95% CI: 0.898−0.942
D
TNFRSF12A
AUC: 0.840
95% CI: 0.822−0.856
E
TNFRSF12A
AUC: 0.819
95% CI: 0.786−0.850
Sensitivity
1 − Specificity
F
Risk, AUC=0.880
ABCA5, AUC=0.597
APOBEC3C, AUC=0.654
EEPD1, AUC=0.372
HEY1, AUC=0.413
IGFBP2, AUC=0.737
RGS14, AUC=0.625
TNFRSF12A, AUC=0.689
G
Risk, AUC=0.911
ABCA5, AUC=0.619
APOBEC3C, AUC=0.675
EEPD1, AUC=0.347
HEY1, AUC=0.377
IGFBP2, AUC=0.774
RGS14, AUC=0.570
TNFRSF12A, AUC=0.702
H
Risk, AUC=0.829
ABCA5, AUC=0.618
APOBEC3C, AUC=0.668
EEPD1, AUC=0.400
HEY1, AUC=0.343
IGFBP2, AUC=0.694
RGS14, AUC=0.605
TNFRSF12A, AUC=0.676
Sensitivity
1−Specificity

Figure 6. Exploration of seven gene signatures in glioma

(A) Correlation analysis among 7 gene signatures and immune cells.

(B and C) ROC curve of IGFBP2 used for predicting the glioma (B) and OS (C).

(D and E) ROC curve of TNFRSF12A used for predicting the glioma (D) and OS (E).

(F–H) ROC curves assessing the discriminating ability of risk and 7 gene signatures in predicting 1- (F), 3- (G) and 5- (H) year OS.

Validation of the transcription levels of 7 signature genes in glioma tissues and normal brain tissues

qRT-PCR further verified that significant differential mRNA expression for the 7 signature genes between glioma tissues and normal brain tissues. the ABCA5 and RGS14 were significantly downregulated in glioma tissues compared with normal brain tissues (all $p < 0.05$), while the APOBEC3C, EEPD1, HEY1, IGFBP2, and TNFRSF12A were significantly upregulated in glioma tissues compared with normal brain tissues (all $p < 0.05$), as predicted by the bioinformatics analysis. (Figures 9A–9G).

TNFRSF12A is highly expressed in glioma

The expression level of TNFRSF12A protein was determined by IHC. As shown in Figure 9H, TNFRSF12A positive staining was mainly located in the cytoplasm and was mainly brown in color. Semi-quantitative analysis showed that the expression rate of TNFRSF12A in glioma was higher than that in non-cancerous brain tissues, and the difference was statistically significant (Figure 9I, $p \leq 0.001$). As shown in Figures 9J and 9K, TNFRSF12A was highly expressed in glioma tissues compared to the corresponding para-tumor tissues. Also, TNFRSF12A was highly expressed in glioma cells compared to normal human astrocytes. (Figures 9L and 9M).

Knockdown of TNFRSF12A suppresses glioma cells proliferation, migration, and invasion *in vitro* and *in vivo*

In order to further explore the function of TNFRSF12A in glioma, a shRNA system was designed to inhibit the TNFRSF12A endogenous expression. Because TNFRSF12A was expressed highest in U87 cells relative to other glioma cells, U87 cells were selected for subsequent experiments. Western blot result showed TNFRSF12A expression was lower in U87-Sh-TNFRSF12A cells than U87-Ctrl cells. (Figures 10A and 10B) The CCK-8 assays indicated that the proliferation of U87-Sh-TNFRSF12A cells was significantly inhibited at 24h, 48h and 72h post-transfection. (Figure 10C) In addition, transwell migration and invasion experiments showed that knock-down of TNFRSF12A weakened the migration and invasion abilities of U87 cells compared with the controls. (Figures 10D–10F).

To further gain insight into the proliferation behavior of TNFRSF12A-modulated glioma cells *in vivo*. As shown in Figures 10G–10I, knock-down of TNFRSF12A expression inhibits glioma growth in the subcutaneous tumor model. In addition, IHC was performed to validate the role of TNFRSF12A in the proliferation of glioma xenografts. The expression level of Ki67, MMP9, and MMP2, some sign of proliferation for tumor malignancy, was higher in control xenografts than that in Sh-TNFRSF12A-xenografts ($p < 0.05$, Figures 10J and 10K). Importantly, it is crucial to note that all experiments were conducted in two groups, including a control group and a TNFRSF12A knockdown group, to ensure the reliability of the findings.

DISCUSSION

The new classification of gliomas by CNS5 combined with internal grading, histological grading and molecular grading has made great progress in the diagnosis and treatment of gliomas.[1] However, due to the huge molecular heterogeneity of gliomas, prognosis and response to therapy still vary considerably from patient to patient. In addition, TME plays an important role in glioma development and treatment resistance. The interaction between TME and tumor cells (including cancer stem cells) further affects the molecular heterogeneity of tumors and affects the invasion and metastasis of tumors.[8,13,14] Therefore, exploring the molecular heterogeneity of glioma, discovering new molecular subtypes and their relationship with TME are very important for finding new therapeutic targets, predicting the prognosis of individual patients, and formulating precise treatment strategies. Worldwide, transcriptional subtyping of glioma has been recognized as a molecular diagnostic method, but the transcriptional subtyping of glioma still needs to be further studied. Therefore, we screened marker genes in gliomas, developed a tumor stratification algorithm, and investigated the association of stratification with TME, patient prognosis, recurrence, and response to immunotherapy.

Firstly, based on the DEGs between glioma and normal tissues, two clusters were identified using an unsupervised clustering algorithm. Significant differences in OS and PFS were found between patients in the two clusters. Subsequently, we further obtained DEGs between the two clusters, and combined with WGCNA, 41 DEGs with significant prognostic correlation were identified. In order to further identify the more valuable signature, we collected 10 widely popular machine learning methods and formed 101 groups and algorithms. Finally, Lasso+RSF was determined to be the best model with the highest average C-index, although RSF obtained the same average C-index. However, considering that Lasso+RSF included fewer variables. We finally selected Lasso+RSF model to construct a risk score.

In 2021, WHO CNS5 updated the molecular markers for different tumor types, which brought more benefits for evaluating patient prognosis and formulating treatment strategies. In addition, TMB, MSI and stem cell index can also be used as a reference for prognosis evaluation.[37,44,45] It is worth noting that our constructed model was predictive independently of these factors. Combined with clinical features, we constructed a Nomogram with high accuracy to predict the 1-, 3-, and 5-year OS of glioma patients. In addition, risk scores were not only significantly correlated with OS and PFS of glioma, but also with TIME, TMB, stem cell index and TIDE, indicating that individual risk scores can predict the prognosis of patients, evaluate the TME and predict the response to immunotherapy. Previous studies have also established

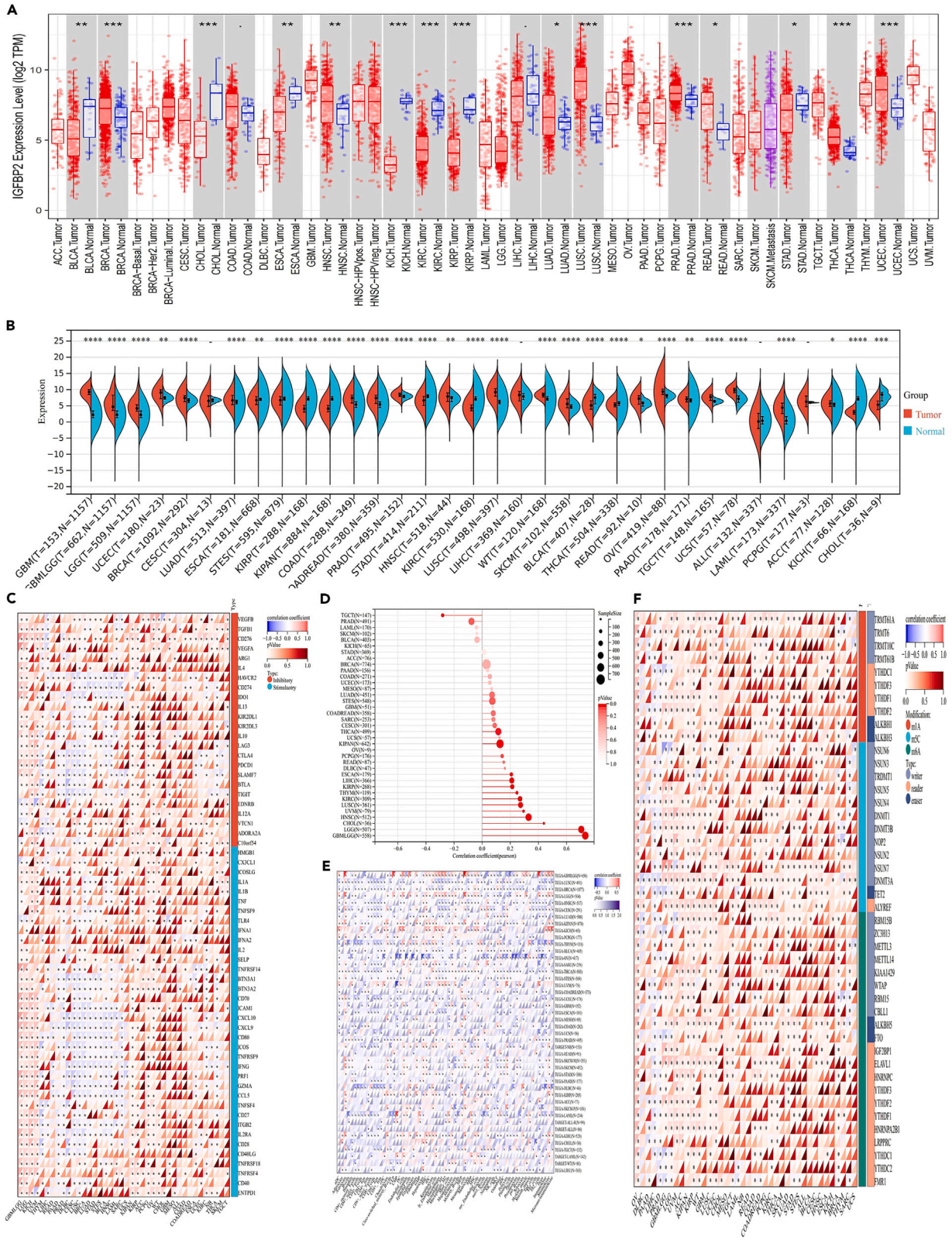
A
IGFBP2 Expression Level (log2 TPM)
ACC.Tumor
BLCA.Tumor
BLCA.Normal
BRCA.Tumor
BRCA.Normal
BRCA−Basal.Tumor
BRCA−Her2.Tumor
BRCA−Luminal.Tumor
CESC.Tumor
CHOL.Tumor
CHOL.Normal
COAD.Tumor
COAD.Normal
DLBC.Tumor
ESCA.Tumor
ESCA.Normal
GBM.Tumor
HNSC.Tumor
HNSC.Normal
HNSC−HPVpos.Tumor
HNSC−HPVneg.Tumor
KICH.Tumor
KICH.Normal
KIRC.Tumor
KIRC.Normal
KIRP.Tumor
KIRP.Normal
LAML.Tumor
LGG.Tumor
LIHC.Tumor
LIHC.Normal
LUAD.Tumor
LUAD.Normal
LUSC.Tumor
LUSC.Normal
MESO.Tumor
OV.Tumor
PAAD.Tumor
PCPG.Tumor
PRAD.Tumor
PRAD.Normal
READ.Tumor
READ.Normal
SARC.Tumor
SKCM.Tumor
SKCM.Metastasis
STAD.Tumor
STAD.Normal
TGCT.Tumor
THCA.Tumor
THCA.Normal
THYM.Tumor
UCEC.Tumor
UCEC.Normal
UCS.Tumor
UVM.Tumor
B
Expression
Group
Tumor
Normal
GBM(T=153,N=1157)
LGG(T=509,N=1157)
UCEC(T=180,N=23)
BRCA(T=1092,N=292)
CESC(T=304,N=13)
LUAD(T=513,N=397)
ESCA(T=181,N=668)
STES(T=595,N=879)
KIRP(T=288,N=168)
KIPAN(T=884,N=168)
COAD(T=288,N=349)
COADREAD(T=380,N=359)
PRAD(T=495,N=152)
STAD(T=414,N=211)
HNSC(T=518,N=44)
KIRC(T=530,N=168)
LUSC(T=498,N=397)
LIHC(T=369,N=160)
WT(T=120,N=168)
SKCM(T=102,N=558)
BLCA(T=407,N=28)
THCA(T=504,N=338)
READ(T=92,N=10)
OV(T=419,N=88)
PAAD(T=178,N=171)
TGCT(T=148,N=165)
UCS(T=57,N=78)
ALL(T=132,N=337)
LAML(T=173,N=337)
PCPG(T=177,N=3)
ACC(T=77,N=128)
KICH(T=66,N=168)
CHOL(T=36,N=9)
C
Type
correlation coefficient
pValue
Inhibitory
Stimulatory
D
SampleSize
pValue
Correlation coefficient(pearson)
E
F
correlation coefficient
pValue
Modification:
m1A
m5C
m6A
Type:
writer
reader
eraser

Figure 7. Prognostic and immune analysis of IGFBP2 in pan-cancer

(A) Expression levels of IGFBP2 in different tumor types in the TCGA database analyzed via TIMER database.

(B) Expression levels of IGFBP2 in different tumor types in the TCGA and GTEx database analyzed via SangerBox website.

(C) The correlation between IGFBP2 expression and immune checkpoint genes in pan-cancer.

(D) The associations between IGFBP2 expression and DNAss in pan-cancer.

(E) The associations between IGFBP2 expression and immune cell infiltration in pan-cancer.

(F) The associations between IGFBP2 expression RNA modification in pan-cancer. *p < 0.05, **p < 0.01, ***p < 0.001. Data are represented as mean ± SEM.

prognostic models for glioma. For example, Shi et al. constructed a prognostic model based on nine ferroptosis-related lncRNAs via the LASSO and Cox analysis.[46] Qu et al. performed univariate and multivariable Cox regression analysis to identified nine m6A-related genes signature to predict the survival probability of glioma patients.[47] Fan et al. used WGCNA and Cox regression analysis to establish an autophagy signature consisting of MUL1, NPC1, and TRIM13.[48] These models facilitate the identification of glioma molecular subtypes. However, we note that these models are not well generalized, our study used more machine learning algorithms for model construction, from which the most accurate one was selected for model construction, and our validation set used multiple cohorts, all of which obtained high C-index values. Therefore, our signature is expected to be a biomarker for evaluating prognosis and guiding the development of treatment strategies for glioma.

In addition, our signature contained seven genes. ABCA5 gene is relatively conserved in evolution,[49,50] which plays an important role in the occurrence of diseases, cholesterol metabolism, and drug resistance.[51–55] ABCA5 can be used as a diagnostic or prognostic biomarker for a variety of diseases, including melanoma, prostate cancer, osteosarcoma, ovarian cancer and childhood acute myeloid leukemia.[56–60] Our study found that high expression of ABCA5 is associated with worse OS and PFS. APOBEC enzymes play an important role in immunity and may contribute to tumorigenesis.[61] Qian et al.[62] found that APOBEC3C was associated with higher kataegis counts and was significantly upregulated in PDAC, and cellular experiments demonstrated the effect of APOBEC3C on PDAC genomes. In addition, they found that APOBEC3C overexpression predicted shorter survival and was associated with CD4 + and CD8 + T lymphocyte invasion, indicating that APOBEC3C enhanced immune activity and validating the utility of APOBEC3C-guided immunotherapy.[54] Our study also confirmed the positive correlation between APOBEC3C and immune cells. EEPD1 is a struct-specific nuclease that promotes the repair of double-ended DSB,[63] which is frequently overexpressed in cancer cells, contributing to the response of tumor cells to oncogenic stress or the development of therapeutic resistance.[64] We found that overexpression of EEPD1 was associated with better OS and DFS in gliomas. HEY1 is an effector gene of Notch signaling pathway.[65] Via immunohistochemistry and immunoblot analysis, Tsung et al.[66] showed that HEY1 was highly expressed in specimens from GBM patients, and HEY1 silencing reduced cell invasion, migration, and proliferation. Moreover, their study provides evidence of a potential positive regulatory loop between HEY1 and p53.[66] A large number of previous studies have shown that IGFBP2 is upregulated in solid tumors, integrates a variety of tumor signaling pathways, and promotes several key carcinogenic processes, such as angiogenesis, transcriptional activation, epithelial-mesenchymal transition, epigenetics, cell migration, cell invasion, tumor stemness and reprogramming, and has become a potential target for tumor therapy.[67–71] Li et al.[67] confirmed the correlation between IGFBP2 and PD-L1, and the combination of IGFBP2 and PD-L1 expression can accurately predict the response to anti-PD-1 therapy in malignant melanoma, and the high expression of IGFBP2 is associated with worse OS and better immune status, which is consistent with our study. More importantly, they revealed a immune-related tumor function in which IGFBP2 promotes EGFR intranuclear accumulation in melanoma cells with subsequent activation of the EGFR/STAT3/PD-L1 signaling pathway.[68] Another study reported that IGFBP2 induced TRIM33 to regulate nuclear β-catenin, which stabilized the binding of cytoplasmic β-catenin to the 3′utr of Oct4 RNA to induce stemness in glioma cells.[69] Our findings showed that IGFBP2 was significantly highly expressed in most cancer types, and these results suggested that IGFBP2 indeed promotes tumorigenesis and tumor progression in human cancer. In addition, IGFBP2 expression was significantly different in different immune subtypes of most cancer types, and this may prove that IGFBP2 is a promising diagnostic pan-cancer biomarker and involved in immune regulation. Our study also found that IGFBP2 was significantly but not always positively correlated with the ESTIMATE score of TME and RNA editing genes in most human cancer types, suggesting that IGFBP2 plays different regulatory roles in various cancer types and is closely related to TME. However, its function needs to be confirmed by further experimental studies. RGS14 can regulate the postsynaptic plasticity of neurons and is crucial for learning, memory and emotion, but its role in glioma has not been studied.[72] Our results suggested that high expression of RGS14 in gliomas may cause poor prognosis. Zhang et al.[73] used CGGA database and GSE43378 dataset to finally identify TNFRSF12A as a biomarker for predicting the prognosis of glioma patients and related to immune cell infiltration. Immunohistochemical staining results verified that TNFRSF12A expression was the lowest in normal brain tissue, followed by low-grade glioma, and the highest in high-grade glioma. To further verify the reliability of our findings, we first verified mRNA expression levels of seven gene signatures in GBM and normal brain tissues by q-PCR, which results are consistent with those of bioinformatic analysis. Subsequently, we focused on the function of TNFRSF12A in glioma. IHC and WB analysis showed that TNFRSF12A protein expression levels in GBM was significantly higher than that of normal brain tissues. In addition, knockdown of TNFRSF12A suppresses glioma cells proliferation, migration, and invasion *in vitro and in vivo*.

Although our model has important clinical implications in glioma, its limitations also exist. First of all, all the samples in this study are from a retrospective study, which needs to be further verified by a well-designed prospective multicenter study in the future. Secondly, our data were derived from public databases, and molecular and clinical information about the samples tested and the patients may have been missing, so it is possible that some critically important characteristics were not considered. Third, the mechanism of action of the seven genes in the model in glioma has not been fully studied, and further *in vitro and in vivo* studies are needed to elucidate their functions in the future. Finally, other omics features were not considered in our model, and multi-omics combination may help to build more powerful models.

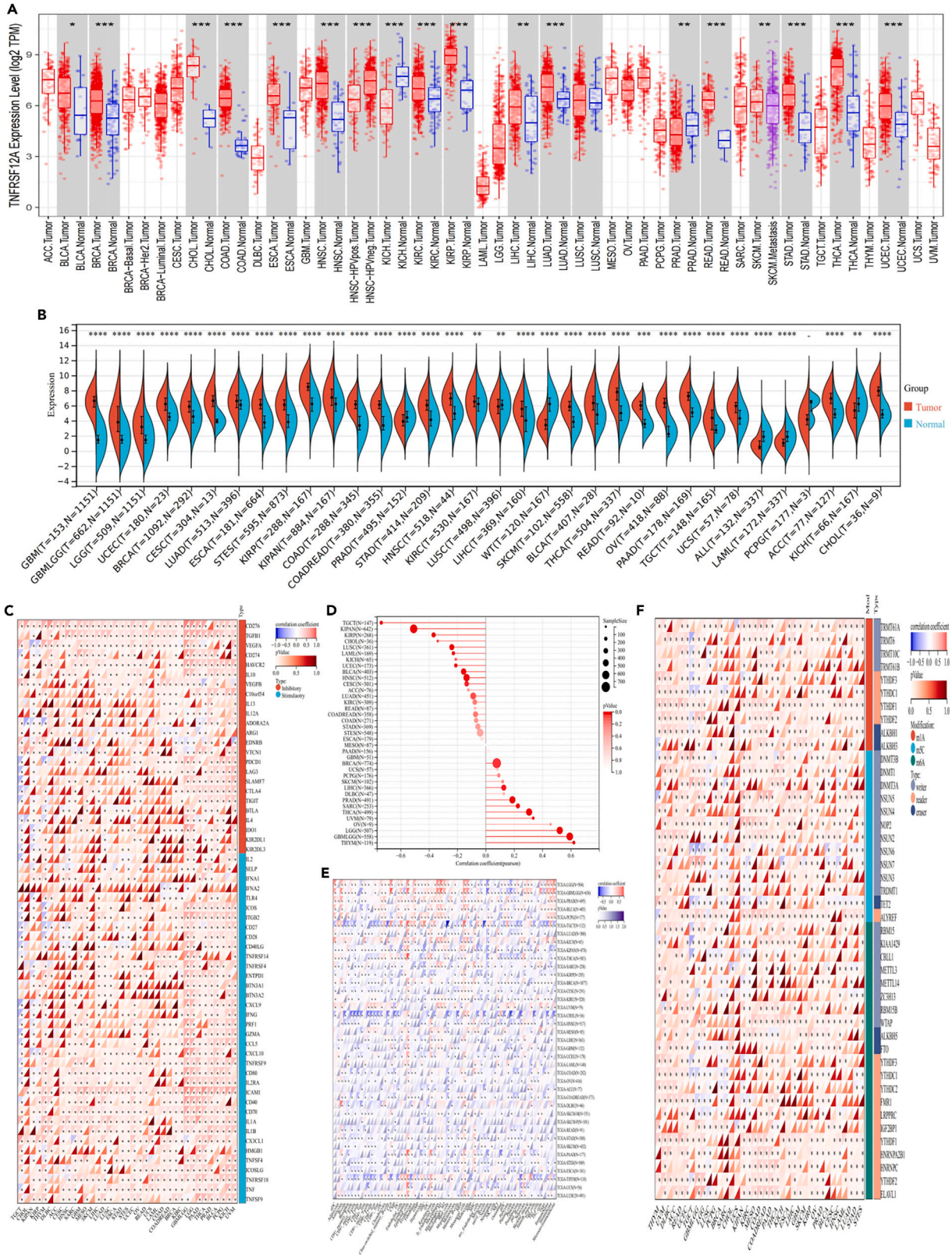
A
TNFRSF12A Expression Level (log2 TPM)
ACC.Tumor
BLCA.Tumor
BLCA.Normal
BRCA.Tumor
BRCA.Normal
BRCA−Basal.Tumor
BRCA−Her2.Tumor
BRCA−Luminal.Tumor
CESC.Tumor
CHOL.Tumor
CHOL.Normal
COAD.Tumor
COAD.Normal
DLBC.Tumor
ESCA.Tumor
ESCA.Normal
GBM.Tumor
HNSC.Tumor
HNSC.Normal
HNSC−HPVpos.Tumor
HNSC−HPVneg.Tumor
KICH.Tumor
KICH.Normal
KIRC.Tumor
KIRC.Normal
KIRP.Tumor
KIRP.Normal
LAML.Tumor
LGG.Tumor
LIHC.Tumor
LIHC.Normal
LUAD.Tumor
LUAD.Normal
LUSC.Tumor
LUSC.Normal
MESO.Tumor
OV.Tumor
PAAD.Tumor
PCPG.Tumor
PRAD.Tumor
PRAD.Normal
READ.Tumor
READ.Normal
SARC.Tumor
SKCM.Tumor
SKCM.Metastasis
STAD.Tumor
STAD.Normal
TGCT.Tumor
THCA.Tumor
THCA.Normal
THYM.Tumor
UCEC.Tumor
UCEC.Normal
UCS.Tumor
UVM.Tumor
B
Expression
Group
Tumor
Normal
GBM(T=153,N=1151)
GBMLGG(T=662,N=1151)
LGG(T=509,N=1151)
UCEC(T=180,N=23)
BRCA(T=1092,N=292)
CESC(T=304,N=13)
LUAD(T=513,N=396)
ESCA(T=181,N=664)
STES(T=595,N=873)
KIRP(T=288,N=167)
KIPAN(T=884,N=167)
COAD(T=288,N=345)
COADREAD(T=380,N=355)
PRAD(T=495,N=152)
STAD(T=414,N=209)
HNSC(T=518,N=44)
KIRC(T=530,N=167)
LUSC(T=498,N=396)
LIHC(T=369,N=160)
WT(T=120,N=167)
SKCM(T=102,N=558)
BLCA(T=407,N=28)
THCA(T=504,N=337)
READ(T=92,N=10)
OV(T=418,N=88)
PAAD(T=178,N=169)
TGCT(T=148,N=165)
UCS(T=57,N=78)
ALL(T=132,N=337)
LAML(T=172,N=337)
PCPG(T=177,N=3)
ACC(T=77,N=127)
KICH(T=66,N=167)
CHOL(T=36,N=9)
C
Type
correlation coefficient
pValue
Type:
Inhibitory
Stimulatory
D
SampleSize
pValue
Correlation coefficient(pearson)
E
correlation coefficient
pValue
F
correlation coefficient
pValue
Modification:
m1A
m5C
m6A
Type:
writer
reader
eraser

Figure 8. Prognostic and immune analysis of TNFRSF12A in pan-cancer

(A) Expression levels of TNFRSF12A in different tumor types in the TCGA database analyzed via TIMER database.

(B) Expression levels of TNFRSF12A in different tumor types in the TCGA and GTEx database analyzed via SangerBox website.

(C) The correlation between TNFRSF12A expression and immune checkpoint genes in pan-cancer.

(D) The associations between TNFRSF12A expression and DNAss in pan-cancer.

(E) The associations between TNFRSF12A expression and immune cell infiltration in pan-cancer.

(F) The associations between TNFRSF12A expression RNA modification in pan-cancer. *$p < 0.05$, **$p < 0.01$, ***$p < 0.001$. Data are represented as mean ± SEM.

In summary, based on bioinformatics and machine learning algorithms, we systematically explored and developed a clinically meaningful signature that can accurately assess the prognosis, recurrence and immunotherapy benefit of glioma patients. This CIPS model has clinical potential to optimize the precision treatment of glioma patients, assist clinical decision-making and find therapeutic targets. In addition, we found that TNFRSF12A promote glioma cells proliferation, migration, and invasion. We also found that the potential of TNFRSF12A and IGFBP2 as a target for anti-tumor immunotherapy.

Limitations of the study

While our study provides valuable insights into glioma subtyping and prognosis prediction, there are notable limitations. The reliance on bioinformatics analyses warrants caution in generalizing findings to diverse datasets or clinical settings. Lack of independent clinical validation, functional experiments, and specific drug response assays limits the immediate translational impact. Heterogeneity within glioma subtypes, potential biases in patient cohorts, and statistical considerations should be acknowledged. Moreover, caution is advised in interpreting predictions related to immunotherapy response without robust experimental validation. These limitations underscore the need for further research and validation to enhance the reliability and clinical applicability of our findings.

STAR★METHODS

Detailed methods are provided in the online version of this paper and include the following:

- KEY RESOURCES TABLE
- RESOURCE AVAILABILITY
  - Lead contact
  - Materials availability
  - Data and code availability
- EXPERIMENTAL MODEL AND STUDY PARTICIPANT DETAILS
  - Tissue preparation
  - Cell culture and transfections
  - Xenograft tumor model
- METHOD DETAILS
  - Data preparation
  - Identification of the glioma subtypes
  - Estimation of TIME of glioma subtypes
  - Construction of weighted correlation network analysis (WGCNA) co-expression network
  - Establishment of signature by machine learning-based integrative approaches
  - Prognostic value of the signature
  - Correlation analysis between TIME and our signature
  - TMB, drug sensitivity analysis and immunotherapy response
  - Exploration of seven gene signatures in glioma
  - Antibodies
  - CCK8 assay
  - Transwell migration and invasion experiments
  - Quantitative real-time PCR
  - Immunohistochemistry (ICH)
- QUANTIFICATION AND STATISTICAL ANALYSIS

SUPPLEMENTAL INFORMATION

Supplemental information can be found online at https://doi.org/10.1016/j.isci.2024.109317.

ACKNOWLEDGMENTS

We sincerely thank the consenting patients, enabling this research. Recognition goes to the Institutional Research Ethics Committee of Guizhou Provincial People's Hospital for approval [Approval Number: (2019)122], emphasizing their dedication to research ethics. Gratitude

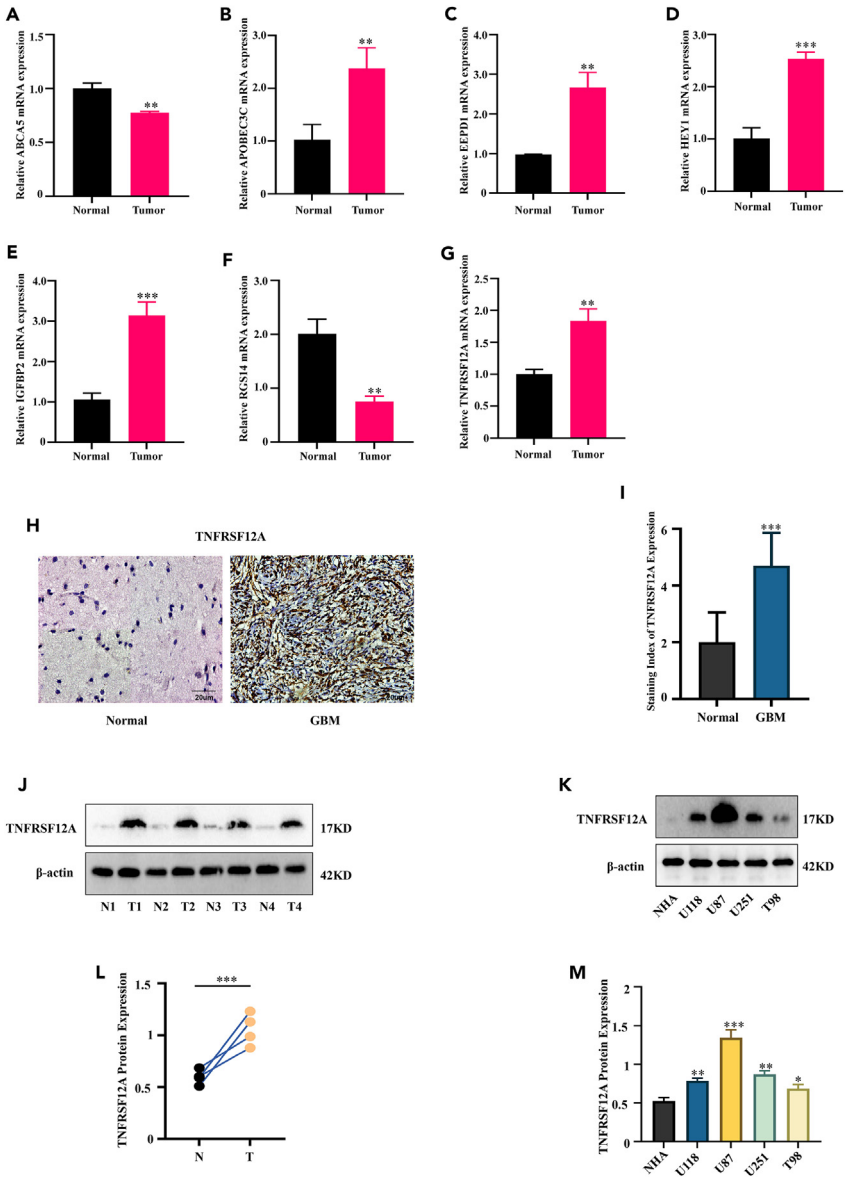

Figure 9. Validation the expression of 7 signature genes and TNFRSF12A protein in glioma tissues and normal brain tissues

(A) ABCA5, (B) APOBEC3C, (C) EEPD1, (D) HEY1, (E) IGFBP2, (F) RGS14, (G) TNFRSF12A expression in normal brain and glioma tissues. *$p < 0.05$; **$p < 0.01$; ***$p < 0.001$.

(H and I) IHC result of TNFRSF12A expression was higher in GBM tissues (GBM) compared to brain tissues (Normal).

(J and K) Western blot result of TNFRSF12A expression was higher in GBM tissues (T) compared to the corresponding para-tumor tissues (N).

(L and M) Western blot result of TNFRSF12A expression in Normal human astrocytes (NHA) and 4 glioma cell lines (U118, U87, U251, T98). (*$p < 0.05$, **$p < 0.01$, ***$p < 0.001$). Data are represented as mean ± SEM.

extends to public database creators and maintainers, notably UCSC Xena (https://tcga.xenahubs.net), CGGA website (http://www.cgga.org.cn/), and GLIOVIS database (http://GLIOVIS.bioinfo.cnio.es/). These databases enriched our study comprehensively. We acknowledge financial support from the National Natural Science Foundation of China (Grants: 82360482, 82260533, 82360376, 81960454, 81960344) and Guizhou Provincial Science and Technology Projects (Grant: [2020]1Z066), vital for our research completion.

AUTHOR CONTRIBUTIONS

S.Y., Y.T., J.Q.Z., and J.L.: Conceptualization. S.Y., X.W., R.Z.H., and M.D.: Data curation, data curation. S.Y., Y.X., L.T., and Z.J.: Investigation, methodology, resources, software. S.Y., Y.X., L.T., and Z.J.: Validation, visualization. S.Y.: Writing–original draft. Y.T., J.Q.Z., and J.L.: Project administration, funding acquisition. All authors: Writing–review and editing.

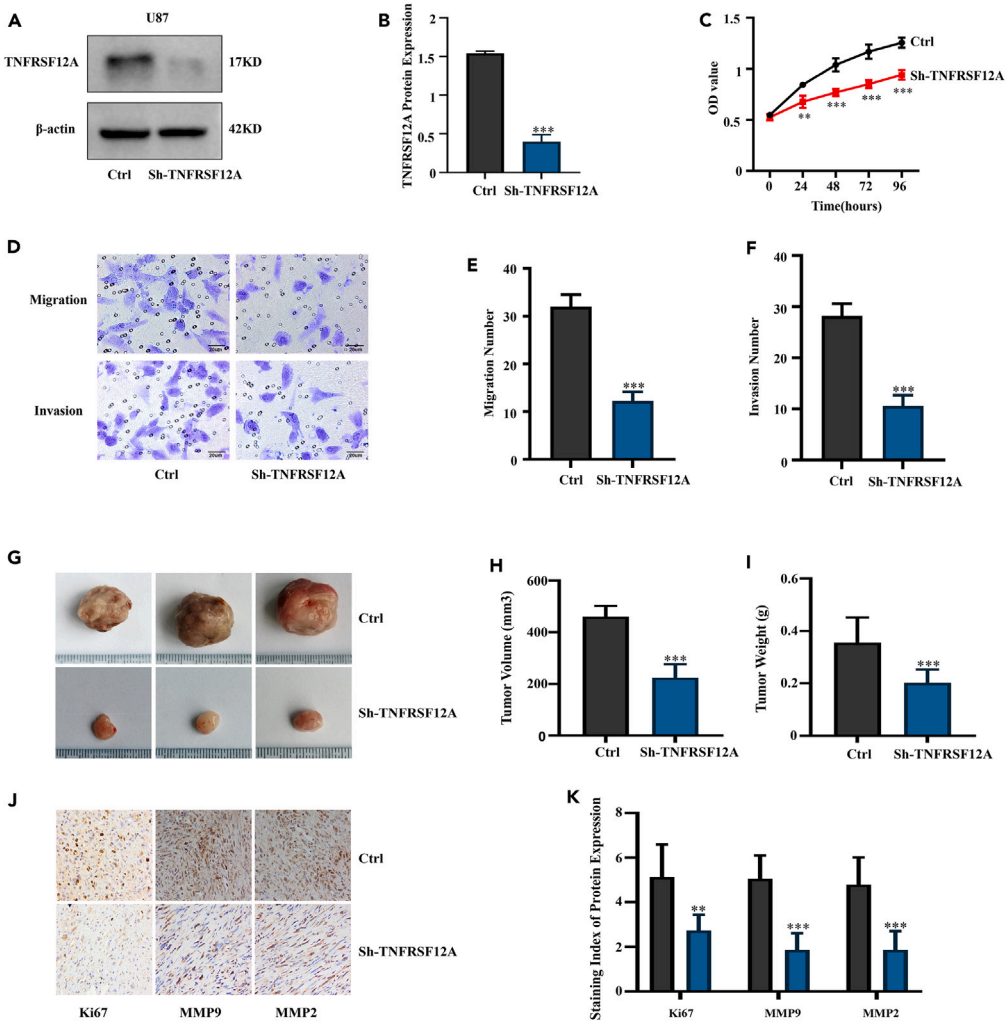

Figure 10. Knockdown of TNFRSF12A suppresses glioma cells proliferation, migration, and invasion *in vitro and in vivo*

(A and B) Western blot analysis of the TNFRSF12A expression in U87-Ctrl cells and U87-Sh-TNFRSF12A cells.

(C) CCK8 assay of knockdown of TNFRSF12A suppresses glioma cell proliferation.

(D–F) Transwell migration and invasion assay of knockdown of TNFRSF12A suppresses glioma cell migration and invasion. (**p < 0.01, ***p < 0.001).

(G) Xenografts produced by U87-Ctrl cells and U87-Sh-TNFRSF12A cells.

(H and I) Knockdown of TNFRSF12A expression inhibits glioma growth in the subcutaneous tumor model.

(J and K) IHC shows knockdown of IGFBP2 suppresses Ki67, MMP9 and MMP2 expression in glioma. (**p < 0.01, ***p < 0.001). Data are represented as mean ± SEM.

DECLARATION OF INTERESTS

The authors declare that they have no competing interests.

Received: September 16, 2023
Revised: January 11, 2024
Accepted: February 17, 2024
Published: February 23, 2024

REFERENCES

1. Louis, D.N., Perry, A., Wesseling, P., Brat, D.J., Cree, I.A., Figarella-Branger, D., Hawkins, C., Ng, H.K., Pfister, S.M., Reifenberger, G., et al. (2021). The 2021 WHO Classification of Tumors of the Central Nervous System: a summary. Neuro Oncol. *23*, 1231–1251. https://doi.org/10.1093/neuonc/noab106.

2. Tan, A.C., Ashley, D.M., López, G.Y., Malinzak, M., Friedman, H.S., and Khasraw, M. (2020). Management of glioblastoma: State of the art and future directions. CA.

Cancer J. Clin. *70*, 299–312. https://doi.org/10.3322/caac.21613.
3. Ostrom, Q.T., Cioffi, G., Gittleman, H., Patil, N., Waite, K., Kruchko, C., and Barnholtz-Sloan, J.S. (2019). CBTRUS Statistical Report: Primary Brain and Other Central Nervous System Tumors Diagnosed in the United States in 2012-2016. Neuro Oncol. *21* (*Suppl 5*), v1–v100. https://doi.org/10.1093/neuonc/noz150.
4. Jooma, R., Waqas, M., and Khan, I. (2019). Diffuse Low-Grade Glioma - Changing Concepts in Diagnosis and Management: A Review. Asian J. Neurosurg. *14*, 356–363. https://doi.org/10.4103/ajns.AJNS_24_18.
5. Weller, M., and Le Rhun, E. (2020). How did lomustine become standard of care in recurrent glioblastoma? Cancer Treat Rev. *87*, 102029. https://doi.org/10.1016/j.ctrv.2020.102029.
6. Jacob, F., Salinas, R.D., Zhang, D.Y., Nguyen, P.T.T., Schnoll, J.G., Wong, S.Z.H., Thokala, R., Sheikh, S., Saxena, D., Prokop, S., et al. (2020). A Patient-Derived Glioblastoma Organoid Model and Biobank Recapitulates Inter- and Intra-tumoral Heterogeneity. Cell *180*, 188–204.e22. https://doi.org/10.1016/j.cell.2019.11.036.
7. Schaff, L.R., and Mellinghoff, I.K. (2023). Glioblastoma and Other Primary Brain Malignancies in Adults: A Review. JAMA *329*, 574–587. https://doi.org/10.1001/jama.2023.0023.
8. Jakola, A.S., Skjulsvik, A.J., Myrmel, K.S., Sjåvik, K., Unsgård, G., Torp, S.H., Aaberg, K., Berg, T., Dai, H.Y., Johnsen, K., et al. (2017). Surgical resection versus watchful waiting in low-grade gliomas. Ann. Oncol. *28*, 1942–1948. https://doi.org/10.1093/annonc/mdx230.
9. van den Bent, M.J., Geurts, M., French, P.J., Smits, M., Capper, D., Bromberg, J.E.C., and Chang, S.M. (2023). Primary brain tumours in adults. Lancet *402*, 1564–1579. https://doi.org/10.1016/S0140-6736(23)01054-1.
10. Weller, M., van den Bent, M., Preusser, M., Le Rhun, E., Tonn, J.C., Minniti, G., Bendszus, M., Balana, C., Chinot, O., Dirven, L., et al. (2021). EANO guidelines on the diagnosis and treatment of diffuse gliomas of adulthood. Nat. Rev. Clin. Oncol. *18*, 170–186. https://doi.org/10.1038/s41571-020-00447-z.
11. McBain, C., Lawrie, T.A., Rogozińska, E., Kernohan, A., Robinson, T., and Jefferies, S. (2021). Treatment options for progression or recurrence of glioblastoma: a network meta-analysis. Cochrane Database Syst. Rev. *5*, CD013579. https://doi.org/10.1002/14651858.CD013579.pub2.
12. He, X., and Xu, C. (2020). Immune checkpoint signaling and cancer immunotherapy. Cell Res. *30*, 660–669. https://doi.org/10.1038/s41422-020-0343-4.
13. Ochocka, N., Segit, P., Walentynowicz, K.A., Wojnicki, K., Cyranowski, S., Swatler, J., Mieczkowski, J., and Kaminska, B. (2021). Single-cell RNA sequencing reveals functional heterogeneity of glioma-associated brain macrophages. Nat. Commun. *12*, 1151. https://doi.org/10.1038/s41467-021-21407-w.
14. Barthel, L., Hadamitzky, M., Dammann, P., Schedlowski, M., Sure, U., Thakur, B.K., and Hetze, S. (2022). Glioma: molecular signature and crossroads with tumor microenvironment. Cancer Metastasis Rev. *41*, 53–75. https://doi.org/10.1007/s10555-021-09997-9.
15. Luis, G., Godfroid, A., Nishiumi, S., Cimino, J., Blacher, S., Maquoi, E., Wery, C., Collignon, A., Longuespée, R., Montero-Ruiz, L., et al. (2021). Tumor resistance to ferroptosis driven by Stearoyl-CoA Desaturase-1 (SCD1) in cancer cells and Fatty Acid Biding Protein-4 (FABP4) in tumor microenvironment promote tumor recurrence. Redox Biol. *43*, 102006. https://doi.org/10.1016/j.redox.2021.102006.
16. Fletcher-Sananikone, E., Kanji, S., Tomimatsu, N., Di Cristofaro, L.F.M., Kollipara, R.K., Saha, D., Floyd, J.R., Sung, P., Hromas, R., Burns, T.C., et al. (2021). Elimination of Radiation-Induced Senescence in the Brain Tumor Microenvironment Attenuates Glioblastoma Recurrence. Cancer Res. *81*, 5935–5947. https://doi.org/10.1158/0008-5472.CAN-21-0752.
17. Bao, Z., Wang, Y., Wang, Q., Fang, S., Shan, X., Wang, J., and Jiang, T. (2021). Intratumor heterogeneity, microenvironment, and mechanisms of drug resistance in glioma recurrence and evolution. Front. Med. *15*, 551–561. https://doi.org/10.1007/s11684-020-0760-2.
18. Zheng, Z., Zhang, J., Jiang, J., He, Y., Zhang, W., Mo, X., Kang, X., Xu, Q., Wang, B., and Huang, Y. (2020). Remodeling tumor immune microenvironment (TIME) for glioma therapy using multi-targeting liposomal codelivery. J. Immunother. Cancer *8*, e000207. https://doi.org/10.1136/jitc-2019-000207.
19. Wang, Q., Hu, B., Hu, X., Kim, H., Squatrito, M., Scarpace, L., deCarvalho, A.C., Lyu, S., Li, P., Li, Y., et al. (2018). Tumor Evolution of Glioma-Intrinsic Gene Expression Subtypes Associates with Immunological Changes in the Microenvironment. Cancer Cell *33*, 152. https://doi.org/10.1016/j.ccell.2017.12.012.
20. Xie, T., Liu, B., Dai, C.G., Lu, Z.H., Dong, J., and Huang, Q. (2019). Glioma stem cells reconstruct similar immunoinflammatory microenvironment in different transplant sites and induce malignant transformation of tumor microenvironment cells. J. Cancer Res. Clin. Oncol. *145*, 321–328. https://doi.org/10.1007/s00432-018-2786-2.
21. Di, W., Fan, W., Wu, F., Shi, Z., Wang, Z., Yu, M., Zhai, Y., Chang, Y., Pan, C., Li, G., et al. (2022). Clinical characterization and immunosuppressive regulation of CD161 (KLRB1) in glioma through 916 samples. Cancer Sci. *113*, 756–769. https://doi.org/10.1111/cas.15236.
22. Hinshaw, D.C., and Shevde, L.A. (2019). The Tumor Microenvironment Innately Modulates Cancer Progression. Cancer Res. *79*, 4557–4566. https://doi.org/10.1158/0008-5472.CAN-18-3962.
23. Eckel-Passow, J.E., Lachance, D.H., Molinaro, A.M., Walsh, K.M., Decker, P.A., Sicotte, H., Pekmezci, M., Rice, T., Kosel, M.L., Smirnov, I.V., et al. (2015). Glioma Groups Based on 1p/19q, IDH, and TERT Promoter Mutations in Tumors. N. Engl. J. Med. *372*, 2499–2508. https://doi.org/10.1056/NEJMoa1407279.
24. Guo, X., Sui, R., and Piao, H. (2023). Exosomes-mediated crosstalk between glioma and immune cells in the tumor microenvironment. CNS Neurosci. Ther. *29*, 2074–2085. https://doi.org/10.1111/cns.14239.
25. Hao, Z., and Guo, D. (2019). EGFR mutation: novel prognostic factor associated with immune infiltration in lower-grade glioma; an exploratory study. BMC Cancer *19*, 1184. https://doi.org/10.1186/s12885-019-6384-8.
26. Dix, A.R., Brooks, W.H., Roszman, T.L., and Morford, L.A. (1999). Immune defects observed in patients with primary malignant brain tumors. J. Neuroimmunol. *100*, 216–232. https://doi.org/10.1016/s0165-5728(99)00203-9.
27. Chen, X., Fan, X., Zhao, C., Zhao, Z., Hu, L., Wang, D., Wang, R., and Fang, Z. (2020). Molecular subtyping of glioblastoma based on immune-related genes for prognosis. Sci. Rep. *10*, 15495. https://doi.org/10.1038/s41598-020-72488-4.
28. Klemm, F., Maas, R.R., Bowman, R.L., Kornete, M., Soukup, K., Nassiri, S., Brouland, J.P., Iacobuzio-Donahue, C.A., Brennan, C., Tabar, V., et al. (2020). Interrogation of the Microenvironmental Landscape in Brain Tumors Reveals Disease-Specific Alterations of Immune Cells. Cell *181*, 1643–1660.e17. https://doi.org/10.1016/j.cell.2020.05.007.
29. Zhong, Q.Y., Fan, E.X., Feng, G.Y., Chen, Q.Y., Gou, X.X., Yue, G.J., and Zhang, G.H. (2019). A gene expression-based study on immune cell subtypes and glioma prognosis. BMC Cancer *19*, 1116. https://doi.org/10.1186/s12885-019-6324-7.
30. Abdelfattah, N., Kumar, P., Wang, C., Leu, J.S., Flynn, W.F., Gao, R., Baskin, D.S., Pichumani, K., Ijare, O.B., Wood, S.L., et al. (2022). Single-cell analysis of human glioma and immune cells identifies S100A4 as an immunotherapy target. Nat. Commun. *13*, 767. https://doi.org/10.1038/s41467-022-28372-y.
31. Le, N.Q.K., Li, W., and Cao, Y. (2023). Sequence-based prediction model of protein crystallization propensity using machine learning and two-level feature selection. Brief. Bioinform. *24*, bbad319. https://doi.org/10.1093/bib/bbad319.
32. Kha, Q.H., Le, V.H., Hung, T.N.K., Nguyen, N.T.K., and Le, N.Q.K. (2023). Development and Validation of an Explainable Machine Learning-Based Prediction Model for Drug-Food Interactions from Chemical Structures. Sensors *23*, 3962. https://doi.org/10.3390/s23083962.
33. Li, S., Zhang, N., Zhang, H., Zhou, R., Li, Z., Yang, X., Wu, W., Li, H., Luo, P., Wang, Z., et al. (2023). Artificial intelligence learning landscape of triple-negative breast cancer uncovers new opportunities for enhancing outcomes and immunotherapy responses. J. Big Data *10*, 132. https://doi.org/10.1186/s40537-023-00809-1.
34. Qin, Y., Deng, J., Zhang, L., Yuan, J., Yang, H., and Li, Q. (2021). Tumor microenvironment characterization in triple-negative breast cancer identifies prognostic gene signature. Aging *13*, 5485–5505. https://doi.org/10.18632/aging.202478.
35. Zhang, H., Zhang, N., Wu, W., Zhou, R., Li, S., Wang, Z., Dai, Z., Zhang, L., Liu, Z., Zhang, J., et al. (2022). Machine learning-based tumor-infiltrating immune cell-associated lncRNAs for predicting prognosis and immunotherapy response in patients with glioblastoma. Brief. Bioinform. *23*, bbac386. https://doi.org/10.1093/bib/bbac386.
36. Zhang, N., Zhang, H., Wu, W., Zhou, R., Li, S., Wang, Z., Dai, Z., Zhang, L., Liu, F., Liu, Z., et al. (2022). Machine learning-based identification of tumor-infiltrating immune cell-associated lncRNAs for improving outcomes and immunotherapy responses in patients with low-grade glioma. Theranostics *12*, 5931–5948. https://doi.org/10.7150/thno.74281.
37. Zhang, H., Dai, Z., Wu, W., Wang, Z., Zhang, N., Zhang, L., Zeng, W.J., Liu, Z., and Cheng, Q. (2021). Regulatory mechanisms of immune

checkpoints PD-L1 and CTLA-4 in cancer. J. Exp. Clin. Cancer Res. *40*, 184. https://doi.org/10.1186/s13046-021-01987-7.
38. Wu, W., Liu, Y., Zeng, S., Han, Y., and Shen, H. (2021). Intratumor heterogeneity: the hidden barrier to immunotherapy against MSI tumors from the perspective of IFN-γ signaling and tumor-infiltrating lymphocytes. J. Hematol. Oncol. *14*, 160. https://doi.org/10.1186/s13045-021-01166-3.
39. Dong, S., Guo, X., Han, F., He, Z., and Wang, Y. (2022). Emerging role of natural products in cancer immunotherapy. Acta Pharm. Sin. B *12*, 1163–1185. https://doi.org/10.1016/j.apsb.2021.08.020.
40. Wang, C., Qiu, J., Chen, S., Li, Y., Hu, H., Cai, Y., and Hou, L. (2021). Prognostic model and nomogram construction based on autophagy signatures in lower grade glioma. J. Cell. Physiol. *236*, 235–248. https://doi.org/10.1002/jcp.29837.
41. Li, G., Wu, F., Zeng, F., Zhai, Y., Feng, Y., Chang, Y., Wang, D., Jiang, T., and Zhang, W. (2021). A novel DNA repair-related nomogram predicts survival in low-grade gliomas. CNS Neurosci. Ther. *27*, 186–195. https://doi.org/10.1111/cns.13464.
42. Zhao, S., Chi, H., Ji, W., He, Q., Lai, G., Peng, G., Zhao, X., and Cheng, C. (2022). A Bioinformatics-Based Analysis of an Anoikis-Related Gene Signature Predicts the Prognosis of Patients with Low-Grade Gliomas. Brain Sci. *12*, 1349. https://doi.org/10.3390/brainsci12101349.
43. Zhou, L., Jiang, Z., Shi, Z., Zhao, W., Lu, Z., Xie, Y., Zhang, B., Lu, H., Tan, G., and Wang, Z. (2021). New Autophagy-Ferroptosis Gene Signature Predicts Survival in Glioma. Front. Cell Dev. Biol. *9*, 739097. https://doi.org/10.3389/fcell.2021.739097.
44. Ge, Y., Gomez, N.C., Adam, R.C., Nikolova, M., Yang, H., Verma, A., Lu, C.P.J., Polak, L., Yuan, S., Elemento, O., and Fuchs, E. (2017). Stem Cell Lineage Infidelity Drives Wound Repair and Cancer. Cell *169*, 636–650.e14. https://doi.org/10.1016/j.cell.2017.03.042.
45. Indraccolo, S., Lombardi, G., Fassan, M., Pasqualini, L., Giunco, S., Marcato, R., Gasparini, A., Candiotto, C., Nalio, S., Fiduccia, P., et al. (2019). Genetic, Epigenetic, and Immunologic Profiling of MMR-Deficient Relapsed Glioblastoma. Clin. Cancer Res. *25*, 1828–1837. https://doi.org/10.1158/1078-0432.CCR-18-1892.
46. Shi, J., Lai, D., Zuo, X., Liu, D., Chen, B., Zheng, Y., Lu, C., and Gu, X. (2022). Identification of Ferroptosis-Related Biomarkers for Prognosis and Immunotherapy in Patients With Glioma. Front. Cell Dev. Biol. *10*, 817643. https://doi.org/10.3389/fcell.2022.817643.
47. Qu, S., Chen, Z., Liu, B., Liu, J., and Wang, H. (2021). N6-methyladenine-related genes affect biological behavior and the prognosis of glioma. Cancer Med. *10*, 98–108. https://doi.org/10.1002/cam4.3574.
48. Fan, Y., Peng, X., Li, B., and Zhao, G. (2020). Development of Autophagy Signature-Based Prognostic Nomogram for Refined Glioma Survival Prognostication. BioMed Res. Int. *2020*, 1872962. https://doi.org/10.1155/2020/1872962.
49. Li, G., Shi, P., and Wang, Y. (2007). Evolutionary dynamics of the ABCA chromosome 17q24 cluster genes in vertebrates. Genomics *89*, 385–391. https://doi.org/10.1016/j.ygeno.2006.07.015.
50. DeStefano, G.M., Kurban, M., Anyane-Yeboa, K., Dall'Armi, C., Di Paolo, G., Feenstra, H., Silverberg, N., Rohena, L., López-Cepeda, L.D., Jobanputra, V., et al. (2014). Mutations in the cholesterol transporter gene ABCA5 are associated with excessive hair overgrowth. PLoS Genet. *10*, e1004333. https://doi.org/10.1371/journal.pgen.1004333.
51. Schumacher, T., and Benndorf, R.A. (2017). ABC Transport Proteins in Cardiovascular Disease-A Brief Summary. Molecules *22*, 589. https://doi.org/10.3390/molecules22040589.
52. Jacobo-Albavera, L., Domínguez-Pérez, M., Medina-Leyte, D.J., González-Garrido, A., and Villarreal-Molina, T. (2021). The Role of the ATP-Binding Cassette A1 (ABCA1) in Human Disease. Int. J. Mol. Sci. *22*, 1593. https://doi.org/10.3390/ijms22041593.
53. Tarling, E.J., de Aguiar Vallim, T.Q., and Edwards, P.A. (2013). Role of ABC transporters in lipid transport and human disease. Trends Endocrinol. Metab. *24*, 342–350. https://doi.org/10.1016/j.tem.2013.01.006.
54. Dean, M., Moitra, K., and Allikmets, R. (2022). The human ATP-binding cassette (ABC) transporter superfamily. Hum. Mutat. *43*, 1162–1182. https://doi.org/10.1002/humu.24418.
55. Briz, O., Perez-Silva, L., Al-Abdulla, R., Abete, L., Reviejo, M., Romero, M.R., and Marin, J.J.G. (2019). What "The Cancer Genome Atlas" database tells us about the role of ATP-binding cassette (ABC) proteins in chemoresistance to anticancer drugs. Expert Opin. Drug Metab. Toxicol. *15*, 577–593. https://doi.org/10.1080/17425255.2019.1631285.
56. Vásquez-Moctezuma, I., Meraz-Ríos, M.A., Villanueva-López, C.G., Magaña, M., Martínez-Macias, R., Sánchez-González, D.J., García-Sierra, F., and Herrera-González, N.E. (2010). ATP-binding cassette transporter ABCB5 gene is expressed with variability in malignant melanoma. Actas Dermosifiliogr. *101*, 341–348. https://doi.org/10.1016/j.ad.2009.12.006.
57. Karatas, O.F., Guzel, E., Duz, M.B., Ittmann, M., and Ozen, M. (2016). The role of ATP-binding cassette transporter genes in the progression of prostate cancer. Prostate *76*, 434–444. https://doi.org/10.1002/pros.23137.
58. Saini, V., Hose, C.D., Monks, A., Nagashima, K., Han, B., Newton, D.L., Millione, A., Shah, J., Hollingshead, M.G., Hite, K.M., et al. (2012). Identification of CBX3 and ABCA5 as putative biomarkers for tumor stem cells in osteosarcoma. PLoS One *7*, e41401. https://doi.org/10.1371/journal.pone.0041401.
59. Hedditch, E.L., Gao, B., Russell, A.J., Lu, Y., Emmanuel, C., Beesley, J., Johnatty, S.E., Chen, X., Harnett, P., George, J., et al. (2014). ABCA transporter gene expression and poor outcome in epithelial ovarian cancer. J. Natl. Cancer Inst. *106*, dju149. https://doi.org/10.1093/jnci/dju149.
60. Niu, P., Yao, B., Wei, L., Zhu, H., Fang, C., and Zhao, Y. (2019). Construction of prognostic risk prediction model based on high-throughput sequencing expression profile data in childhood acute myeloid leukemia. Blood Cells Mol. Dis. *77*, 43–50. https://doi.org/10.1016/j.bcmd.2019.03.008.
61. Revathidevi, S., Murugan, A.K., Nakaoka, H., Inoue, I., and Munirajan, A.K. (2021). APOBEC: A molecular driver in cervical cancer pathogenesis. Cancer Lett. *496*, 104–116. https://doi.org/10.1016/j.canlet.2020.10.004.
62. Qian, Y., Gong, Y., Zou, X., Liu, Y., Chen, Y., Wang, R., Dai, Z., Tasiheng, Y., Lin, X., Wang, X., et al. (2022). Aberrant APOBEC3C expression induces characteristic genomic instability in pancreatic ductal adenocarcinoma. Oncogenesis *11*, 35. https://doi.org/10.1038/s41389-022-00411-9.
63. Wu, Y., Lee, S.H., Williamson, E.A., Reinert, B.L., Cho, J.H., Xia, F., Jaiswal, A.S., Srinivasan, G., Patel, B., Brantley, A., et al. (2015). EEPD1 Rescues Stressed Replication Forks and Maintains Genome Stability by Promoting End Resection and Homologous Recombination Repair. PLoS Genet. *11*, e1005675. https://doi.org/10.1371/journal.pgen.1005675.
64. Nickoloff, J.A., Sharma, N., Taylor, L., Allen, S.J., Lee, S.H., and Hromas, R. (2022). Metnase and EEPD1: DNA Repair Functions and Potential Targets in Cancer Therapy. Front. Oncol. *12*, 808757. https://doi.org/10.3389/fonc.2022.808757.
65. Sahu, A., Devi, S., Jui, J., and Goldman, D. (2021). Notch signaling via Hey1 and Id2b regulates Müller glia's regenerative response to retinal injury. Glia *69*, 2882–2898. https://doi.org/10.1002/glia.24075.
66. Tsung, A.J., Guda, M.R., Asuthkar, S., Labak, C.M., Purvis, I.J., Lu, Y., Jain, N., Bach, S.E., Prasad, D.V.R., and Velpula, K.K. (2017). Methylation regulates HEY1 expression in glioblastoma. Oncotarget *8*, 44398–44409. https://doi.org/10.18632/oncotarget.17897.
67. Li, T., Forbes, M.E., Fuller, G.N., Li, J., Yang, X., and Zhang, W. (2020). IGFBP2: integrative hub of developmental and oncogenic signaling network. Oncogene *39*, 2243–2257. https://doi.org/10.1038/s41388-020-1154-2.
68. Sun, L., Zhang, X., Song, Q., Liu, L., Forbes, E., Tian, W., Zhang, Z., Kang, Y., Wang, H., Fleming, J.B., et al. (2021). IGFBP2 promotes tumor progression by inducing alternative polarization of macrophages in pancreatic ductal adenocarcinoma through the STAT3 pathway. Cancer Lett. *500*, 132–146. https://doi.org/10.1016/j.canlet.2020.12.008.
69. Wei, L.F., Weng, X.F., Huang, X.C., Peng, Y.H., Guo, H.P., and Xu, Y.W. (2021). IGFBP2 in cancer: Pathological role and clinical significance (Review). Oncol. Rep. *45*, 427–438. https://doi.org/10.3892/or.2020.7892.
70. Wang, J., Chen, Y., Zeng, Z., Feng, R., Wang, Q., Zhang, Q., Sun, K., Chen, A.F., Lu, Y., and Yu, Y. (2021). HMGA2 contributes to vascular development and sprouting angiogenesis by promoting IGFBP2 production. Exp. Cell Res. *408*, 112831. https://doi.org/10.1016/j.yexcr.2021.112831.
71. Verma, B.K., and Kondaiah, P. (2020). Regulation of β-catenin by IGFBP2 and its cytoplasmic actions in glioma. J. Neuro Oncol. *149*, 209–217. https://doi.org/10.1007/s11060-020-03596-4.
72. Harbin, N.H., Bramlett, S.N., Montanez-Miranda, C., Terzioglu, G., and Hepler, J.R. (2021). RGS14 Regulation of Post-Synaptic Signaling and Spine Plasticity in Brain. Int. J. Mol. Sci. *22*, 6823. https://doi.org/10.3390/ijms22136823.
73. Zhang, Y., Yang, X., Zhu, X.L., Wang, Z.Z., Bai, H., Zhang, J.J., Hao, C.Y., and Duan, H.B. (2021). A Novel Immune-Related Prognostic Biomarker and Target Associated With Malignant Progression of Glioma. Front. Oncol. *11*, 643159. https://doi.org/10.3389/fonc.2021.643159.
74. Zhao, S., Ye, Z., and Stanton, R. (2020). Misuse of RPKM or TPM normalization when

comparing across samples and sequencing protocols. RNA *26*, 903–909. https://doi.org/10.1261/rna.074922.120.

75. Leek, J.T., Johnson, W.E., Parker, H.S., Jaffe, A.E., and Storey, J.D. (2012). The sva package for removing batch effects and other unwanted variation in high-throughput experiments. Bioinformatics *28*, 882–883. https://doi.org/10.1093/bioinformatics/bts034.
76. Ringnér, M. (2008). What is principal component analysis? Nat. Biotechnol. *26*, 303–304. https://doi.org/10.1038/nbt0308-303.
77. Ritchie, M.E., Phipson, B., Wu, D., Hu, Y., Law, C.W., Shi, W., and Smyth, G.K. (2015). limma powers differential expression analyses for RNA-sequencing and microarray studies. Nucleic Acids Res. *43*, e47. https://doi.org/10.1093/nar/gkv007.
78. Wilkerson, M.D., and Hayes, D.N. (2010). ConsensusClusterPlus: a class discovery tool with confidence assessments and item tracking. Bioinformatics *26*, 1572–1573. https://doi.org/10.1093/bioinformatics/btq170.
79. Hänzelmann, S., Castelo, R., and Guinney, J. (2013). GSVA: gene set variation analysis for microarray and RNA-seq data. BMC Bioinf. *14*, 7. https://doi.org/10.1186/1471-2105-14-7.
80. Ashburner, M., Ball, C.A., Blake, J.A., Botstein, D., Butler, H., Cherry, J.M., Davis, A.P., Dolinski, K., Dwight, S.S., Eppig, J.T., et al. (2000). Gene ontology: tool for the unification of biology. The Gene Ontology Consortium. Nat. Genet. *25*, 25–29. https://doi.org/10.1038/75556.
81. Kanehisa, M., Furumichi, M., Tanabe, M., Sato, Y., and Morishima, K. (2017). KEGG: new perspectives on genomes, pathways, diseases and drugs. Nucleic Acids Res. *45*, D353–D361. https://doi.org/10.1093/nar/gkw1092.
82. Wu, T., Hu, E., Xu, S., Chen, M., Guo, P., Dai, Z., Feng, T., Zhou, L., Tang, W., Zhan, L., et al. (2021). clusterProfiler 4.0: A universal enrichment tool for interpreting omics data. Innovation *2*, 100141. https://doi.org/10.1016/j.xinn.2021.100141.
83. Langfelder, P., and Horvath, S. (2008). WGCNA: an R package for weighted correlation network analysis. BMC Bioinf. *9*, 559. https://doi.org/10.1186/1471-2105-9-559.
84. Heagerty, P.J., Lumley, T., and Pepe, M.S. (2000). Time-dependent ROC curves for censored survival data and a diagnostic marker. Biometrics *56*, 337–344. https://doi.org/10.1111/j.0006-341x.2000.00337.x.
85. Vickers, A.J., Van Calster, B., and Steyerberg, E.W. (2016). Net benefit approaches to the evaluation of prediction models, molecular markers, and diagnostic tests. BMJ *352*, i6. https://doi.org/10.1136/bmj.i6.
86. Geeleher, P., Cox, N., and Huang, R.S. (2014). pRRophetic: an R package for prediction of clinical chemotherapeutic response from tumor gene expression levels. PLoS One *9*, e107468. https://doi.org/10.1371/journal.pone.0107468.
87. Tang, Z., Kang, B., Li, C., Chen, T., and Zhang, Z. (2019). GEPIA2: an enhanced web server for large-scale expression profiling and interactive analysis. Nucleic Acids Res. *47*, W556–W560. https://doi.org/10.1093/nar/gkz430.
88. Li, T., Fan, J., Wang, B., Traugh, N., Chen, Q., Liu, J.S., Li, B., and Liu, X.S. (2017). TIMER: A Web Server for Comprehensive Analysis of Tumor-Infiltrating Immune Cells. Cancer Res. *77*, e108–e110. https://doi.org/10.1158/0008-5472.CAN-17-0307.
89. Wang, D., Wang, Y., Zou, X., Shi, Y., Liu, Q., Huyan, T., Su, J., Wang, Q., Zhang, F., Li, X., and Tie, L. (2020). FOXO1 inhibition prevents renal ischemia-reperfusion injury via cAMP-response element binding protein/PPAR-γ coactivator-1α-mediated mitochondrial biogenesis. Br. J. Pharmacol. *177*, 432–448. https://doi.org/10.1111/bph.14878.
90. Danilova, L., Ho, W.J., Zhu, Q., Vithayathil, T., De Jesus-Acosta, A., Azad, N.S., Laheru, D.A., Fertig, E.J., Anders, R., Jaffee, E.M., and Yarchoan, M. (2019). Programmed Cell Death Ligand-1 (PD-L1) and CD8 Expression Profiling Identify an Immunologic Subtype of Pancreatic Ductal Adenocarcinomas with Favorable Survival. Cancer Immunol. Res. *7*, 886–895. https://doi.org/10.1158/2326-6066.CIR-18-0822.
91. Malta, T.M., Sokolov, A., Gentles, A.J., Burzykowski, T., Poisson, L., Weinstein, J.N., Kamińska, B., Huelsken, J., Omberg, L., Gevaert, O., et al. (2018). Machine Learning Identifies Stemness Features Associated with Oncogenic Dedifferentiation. Cell *173*, 338–354.e15. https://doi.org/10.1016/j.cell.2018.03.034.
92. Yoshihara, K., Shahmoradgoli, M., Martínez, E., Vegesna, R., Kim, H., Torres-Garcia, W., Treviño, V., Shen, H., Laird, P.W., Levine, D.A., et al. (2013). Inferring tumour purity and stromal and immune cell admixture from expression data. Nat. Commun. *4*, 2612. https://doi.org/10.1038/ncomms3612.
93. Aran, D., Hu, Z., and Butte, A.J. (2017). xCell: digitally portraying the tissue cellular heterogeneity landscape. Genome Biol. *18*, 220. https://doi.org/10.1186/s13059-017-1349-1.
94. Ru, B., Wong, C.N., Tong, Y., Zhong, J.Y., Zhong, S.S.W., Wu, W.C., Chu, K.C., Wong, C.Y., Lau, C.Y., Chen, I., et al. (2019). TISIDB: an integrated repository portal for tumor-immune system interactions. Bioinformatics *35*, 4200–4202. https://doi.org/10.1093/bioinformatics/btz210.

STAR★METHODS

KEY RESOURCES TABLE

REAGENT or RESOURCE	SOURCE	IDENTIFIER
Antibodies		
TNFRSF12A	Abcam	ab109365; RRID: AB_1858463
MMP9	Abcam	ab76003; RRID: AB_854905
MMP2	Abcam	ab92536; RRID: AB_854897
Ki67	Abcam	ab16667; RRID: AB_2722785
β-actin	Abcam	ab8226; RRID: AB_2750915
HPR-conjugated secondary antibodies	CST	#58802; #5127; RRID: AB_2371065
Chemicals, peptides, and recombinant proteins		
DMEM	Gibco	C11995500BT
FBS	Gibco	#12664025C
Penicillin/streptomycin	Beyotime	# C0222
Polybrene	Solarbio	# C0351
pLKO.3G	Addgene	# 14748
RNAiso Plus	TaKaRa	# 9108Q
RIPA Lysis Buffer	Beyotime	# P0013B
Polyvinylidene difluoride membrane	Millipore	# 3010040001
BSA	Beyotime	# ST025
Crystal violet	Beyotime	# C0121
Matrigel	BD	# 354234
24-well Transwell chambers	Corning	# 3473
Critical commercial assays		
Primescript RT reagent Kit	TaKaRa	# RR047Q
Chemiluminescent detection kit	Millipore	#WBAVDCH01
CCK-8 assay	Beyotime	# C0046
Experimental models: Cell lines		
T98 cell line	Procell Life Science &Technology	# CL-0583
U251 cell line	Procell Life Science &Technology	# CL-0237
U118 cell line	Chinese Academy of Sciences Cell Bank	# TCHu216
U87 cell line	Chinese Academy of Sciences Cell Bank	# TCHu138
Experimental models: Organisms/strains		
BALB/c nude mice	Tengxin	N/A
Oligonucleotides		
ABCA5	Sangon Biotech	N/A
F: 5′-GCTTCCAGAACCACCAGACA-3′		
R: 5′- TCACAACACTGGCAACCCAT-3′		
APOBEC3C	Sangon Biotech	N/A
F: 5′- CAGGCACAGCAACGTGAATC-3′		
R: 5′- GGAGCCCCTCCTGGTAACAT-3′		
EEPD1	Sangon Biotech	N/A
F: 5′- GGGAGGTTCAAGGTGGGAAG-3′		
R:5′- TAGGGTCTGTGCAAAGCTCG-3′		
HEY1	Sangon Biotech	N/A

(*Continued on next page*)

Continued

REAGENT or RESOURCE	SOURCE	IDENTIFIER
F: 5′- GGCTGGTACCCAGTGCTTTT-3′		
R: 5′- GGTCATCTGCAGGATCTCGG-3′		
IGFBP2	Sangon Biotech	N/A
F: 5′- GCTGGTCATGGGCGAGG-3′		
R: 5′-CCAGCTCCTTCATACCCGAC-3′		
TNFRSF12A	Sangon Biotech	N/A
F:5′-CTCTGAGCCTGACCTTCGTG-3′		
R: 5′-GTCTCCTCTATGGGGGTGGT-3′		
GAPDH	Sangon Biotech	N/A
F: 5′-TTCCAGCCTTCCTTCCTGGG-3′		
R: 5′-TTGCGCTCAGGAGGAGCAAT-3′		
Software and algorithms		
GraphPad Prism 9	GraphPad	https://www.graphpad.com/
SPSS 23.0	SPSS	http://www.spss.com.cn
Image J	National Institutes of Health	https://imagej.nih.gov/ij
R(v4.1.3)	The R Project	https://www.r-project.org
sva	(Leek JT et al.)	https://bioconductor.org/packages/release/bioc/html/sva.html
limma	(Ritchie et al.)	https://bioconductor.org/packages/release/bioc/html/limma.html
ConsensusClusterPlus	(Wilkerson et al.)	https://bioconductor.org/packages/release/bioc/html/ConsensusClusterPlus.html
GSVA	(Hänzelmann et al.)	https://bioconductor.org/packages/release/bioc/html/GSVA.html
clusterProfiler	(Wu et al.)	https://bioconductor.org/packages/release/bioc/html/clusterProfiler.html
WGCNA	(Langfelder et al.)	https://horvath.genetics.ucla.edu/html/CoexpressionNetwork/Rpackages/WGCNA/
survivalROC	(Heagerty et al.)	https://rdocumentation.org/packages/survivalROC/versions/1.0.3.1
ML		Data S2

RESOURCE AVAILABILITY

Lead contact

Further information and requests for resources and reagents should be directed to and will be fulfilled by the Lead Contact, Ying Tan (tanyinggz5055@163.com).

Materials availability

This study did not generate new unique reagents.

Data and code availability

Data

Public data used in this work can be acquired from the UCSC Xena (https://tcga.xenahubs.net), CGGA website (http://www.cgga.org.cn/), GLIOVIS database (http://GLIOVIS.bioinfo.cnio.es/), and GEO databases (https://www.ncbi.nlm.nih.gov/geo/).

Code

This study does not report original code. Most codes were used in this study in alignment with recommendations made by authors of R packages in their respective user's guide, which can be accessed at https://bioconductor.org. Other code is available in this paper's supplemental information.

Additional information requests

Any additional information required to reanalyze the data used in this study is available from the lead contact upon request.

Availability of data and materials

Publicly available datasets were analyzed in this study. These data can be found here: UCSC Xena; CGGA website; GLIOVIS database; GEO databases.

EXPERIMENTAL MODEL AND STUDY PARTICIPANT DETAILS

Tissue preparation

For immunohistochemistry, twelve glioblastomas (GBM) and twelve brain were obtained from the Guizhou Provincial People's Hospital. For western blot analysis, 4 GBM tissues and the corresponding para-tumor tissues were also obtained. The study was approved by the Ethics Committee of Guizhou Provincial People's Hospital, China. All patients approved informed consents.

Cell culture and transfections

Two GBM cell lines (U118 and U87) were purchased from the Chinese Academy of Sciences Cell Bank (Shanghai, China), while GBM cell lines T98 and U251 from Procell Life Science &Technology (Wuhan, China). Above four GBM cell lines were cultured in DMEM (Gibco, USA) supplemented with 10% fetal bovine serum (FBS, Gibco, USA) and 1% penicillin/streptomycin (Beyotime, China) at 37°C with 5% CO2. For transduction, U118 cell lines were maintained at 60% confluence in six-well plates, and viral solutions were added into a cell culture medium that contains 8 μg/mL polybrene (Solarbio, China), then selected using neomycin (Beyotime, China). Endogenous TNFRSF12A was knocked down using an shRNA system (pLKO.3G from Addgene). The target sequence is GAAGTTCACCACCCCCATAGA.

Xenograft tumor model

Male nude mice (4 weeks old) sourced from the Experimental Animal Center of Guizhou provincial people's hospital were employed in this study, following approval by the Ethics Committee of Guizhou provincial people's hospital for all animal-related procedures. Glioma cells, resuspended in DMEM at a density of 2×10^6 cells per 50 μl, were subcutaneously injected into the nude mice. Following a 28-day period, the mice were euthanized, and the tumor tissues were excised and weighed. Subsequently, the excised tumor tissues were utilized for immunohistochemistry analysis.

METHOD DETAILS

Data preparation

The RNA-Seq (RNA SeqV2 RSEM) and clinical annotations for 153 GBM and 509 LGG samples from TCGA and 1152 normal brain samples from GTEx project were obtained from a combined set of TCGA and GTEx samples in UCSC Xena (https://tcga.xenahubs.net), which were set as a training cohort. Normalized gene expression was measured as transcripts per kilobase million (TPM) values.[74] The Chinese Glioma Genome Atlas (CGGA) platform were choiced to acquire CGGA-325 and CGGA-693 with detailed transcriptomic data and clinical information (http://www.cgga.org.cn/). Microarray data and clinical information of glioma samples of Gravendeel cohort, Rembrant cohort, and Gravendeel cohort were obtained from GLIOVIS database (http://GLIOVIS.bioinfo.cnio.es/). The samples from CGGA and GLIOVIS database were merged as a meta data to be validation cohorts by utilizing sva R package for the normalization of RNA expression profiles and removal of batch effect.[75] In addition, GSE7696, GSE42670, GSE43378, GSE50021, GSE72951, and GSE83300 including glioma data were retrieved from GEO databases (https://www.ncbi.nlm.nih.gov/geo/), which were merged as a meta data to be test cohorts by utilizing sva R package. We plotted PCA plots of the data before and after normalization and batch effect removal to visually demonstrate the treatment effect.[76]

Identification of the glioma subtypes

First, limma R packages was used to analyze differentially expressed genes (DEGs) between the glioma and normal brain samples in training cohort (adjusted P-values < 0.05 and |log2-FC| >1).[77] Then, we performed k-means consensus clustering to distinguish different molecular subtypes based on the mRNA expression profiles of all DEGs by using ConsensusClusterPlus R package with 1000 repetitions.[78] Kaplan-Meier (K-M) plot was draw to reveal differences in OS and PFS of glioma between subtypes with a log-rank significance test.

Estimation of TIME of glioma subtypes

Single-sample gene set enrichment analysis (ssGSEA) implemented was employed to quantify the relative infiltration of 28 immune cells in training cohorts using GSVA R package.[79] To verify the stability and robustness of the ssGSEA results, seven other algorithms including TIMER, CIBERSORT, CIBERSORT−ABS, QUANTISEQ, MCPCOUNTER, XCELL, and EPIC, were further performed to quantify infiltration of immune cells in the training cohorts. GSVA was performed to explore the activity variation of pathways in each subtype by using GSVA R package, while the "c2.cp.kegg.v7.2.symbols. gmt" gene sets were used as the reference gene set. Then Gene ontology (GO)[80] and Kyoto Encyclopedia of Genes and Genomes (KEGG)[81] enrichment analyses were completed based on the DEGs between glioma subtypes using clusterProfiler R package.[82]

Construction of weighted correlation network analysis (WGCNA) co-expression network

Co-expression gene networks of glioma patients were constructed via WGCNA by using WGCNA R package.[83] Using the scale-free topological model, the soft threshold parameter β was the best to meet the criteria of scale-free network when it was fitted to 0.9. Then, the weighted adjacency matrix is transformed into topological overlap measure (TOM) to calculate the degree of association between genes and generate the distTOM (1-TOM). The dynamic tree cutting method was used for module identification. After gene modules were established, different modules were distinguished by color, and modules with high similarity were merged. The module feature genes were clustered and merged after the completion of clustering.

To identify the modules with the strongest correlation with tumor subtypes, Pearson correlation analysis was used. Finally, gene significance (GS) and module membership (MM) values were obtained to select genes highly related to tumor immune subtypes.

Establishment of signature by machine learning-based integrative approaches

The intersection of DEGs between glioma subtypes and hub genes screened by WGCNA was obtained for Univariate Cox analysis. The genes possessing an adjusted $P < 0.05$ were selected for further investigation. Subsequently, we combined 10 machine learning algorithms,included Lasso, Ridge, CoxBoost, stepwise Cox, random survival forest (RSF), partial least squares regression for Cox (plsRcox), elastic network (Enet), survival support vector machine (survival-SVM), generalised boosted regression modelling (GBM), and supervised principal components (SuperPC), to generate a consensus model. And then, 101 algorithm combinations were performed on prognostic genes to fit prediction models based on the 10-fold cross-validation framework in training cohort to develop a consensus signature with stability performance and high accuracy. The validation cohorts, including CGGA-325, CGGA-693, Gravendeel, Rembrant, and Gravendeel cohort were used to detect all models. For each model, the C-indices across all datasets were calculated. Finally, The most optimal signature was screened out in the model with the highest average C-index.

Prognostic value of the signature

The risk score for each glioma patients was calculated based on optimal model. The glioma patients in the all cohorts were classified into low-risk subgroup and high-risk subgroup based on the median of risk score calculated in training cohort. Moreover, survival analysis for Overall Survival (OS) and Progression Free Survival (PFS) was conducted to explore the prognostic value of the risk score. Next, combining clinical annotation information and risk scores, we identified independent prognostic factors by univariate and multivariate Cox regression analyses. A nomogram predicting the probability of overall survival at 1, 3, 5 years was draw by rms R package. The time-dependent receiver operating characteristic (ROC) curve analysis was performed, and 1-, 3-, 5- years the area under the curve (AUC) was calculated to verify the prognosis of glioma patients by using survivalROC R package.[84] Moreover, the calibration plot was used to determine the prediction accuracy of our model.

To rigorously compare the prognostic predictive capabilities of our glioblastoma model with other established models at 1, 3, 5, and 8 years, we computed decision curve analysis (DCA) and the concordance index (C-index) based on TCGA data.[85] In the ROC curve analysis, we plotted the sensitivity against 1-specificity at various threshold levels for each model and calculated the AUC at 1, 3, 5, and 8 years to evaluate accuracy. The C-index was calculated for each model across these time horizons to assess their predictive discrimination capabilities. We also evaluated the clinical utility of each model by analyzing the net benefits at different threshold probabilities at the specified time points through DCA.

Correlation analysis between TIME and our signature

Eight algorithms including ssGSEA, TIMER, CIBERSORT, CIBERSORT−ABS, QUANTISEQ, MCPCOUNTER, XCELL, and EPIC, was employed to quantify the difference of relative infiltration of immune cells between high-risk and low-risk subgroups. The expression of checkpoints between high-risk and low-risk subgroups was also calculated. To demonstrate that risk scores could reflect heterogeneity among tumors, we investigated whether risk scores differed among previously defined tumor immune subtypes. The six distinct immune subtypes include: C1 (wound healing); C2 (IFN-gamma dominant); C3 (inflammatory); C4 (lymphocyte depleted); C5 (immunologically quiet); C6 (TGF-b dominant). To further explore the immunological relevance of the gene signature, we also drew a heatmap of the correlation between each gene used to construct the model and immune cells.

TMB, drug sensitivity analysis and immunotherapy response

TMB have been proved to be important biomarkers of the TME.[45] Thus, the correlations between the TMB of TCGA cohort and riskscore was evaluated. Then Kaplan–Meier analysis was used to compared OS between high-TMB and low-TMB group, which were classiffied by median value of TMB, and to compared OS among the four groups, including high-TMB-high-risk, high-TMB-low-risk, low-TMB-high-risk and low-TMB-low-risk. In addition, we used the pRRophetic R package to assessed drug-response prediction by predicting half-maximum inhibitory concentration (IC50) of drugs in each sample.[86] Furthermore, we performed Tumor Immune Dysfunction and Exclusion (TIDE) algorithm (http://tide.dfci.harvard.edu/) to predict potential response to immunotherapy of glioma patients. The higher TIDE score, the worse response to immunotherapy.

Exploration of seven gene signatures in glioma

The GEPIA database (http://gepia2.cancer-pku.cn/) were used to explore the prognostic value of seven gene expression in glioma.[87] AUC was calculated to explore the value of seven gene for distinguishing glioma and normal brain tissue, risk of glioma patients. TIMER database

(https://cistrome.shinyapps.io/timer/), and SangerBox website (http://sangerbox.com/Tool), were used to compare IGFBP2 expression between human cancers and paired normal tissue.[88,89] Correlations between IGFBP2 expression and immune checkpoint (ICP) genes, tumor stemness score, ESTIMATE score, and xCell scores in the TME was explored via the SangerBox website.[90–93] We also explored the correlation between IGFBP2 expression and RNA modification, including m1A, m5C, and m6A in the TME of human cancer. The TISIDB database (http://cis.hku.hk/TISIDB/index.php) was used to explore correlations between IGFBP2 expression and immune subtypes of different cancer types.[94]

Antibodies

TNFRSF12A, MMP9, MMP2, and Ki67 antibodies were obtained from Abcam (UK); HPR-conjugated secondary antibodies were purchased from Cell Signaling Technology (USA).

CCK8 assay

Cell proliferation ability was determined by CCK-8 assay (Beyotime, China), with each experimental condition replicated five times. Glioma cells were seeded and cultured in a 96-well microplate at a density of 5000 cells/well. After the addition of 10 μL of CCK-8 reagent in each well, glioma cells were incubated at 37°C for 1 h. The absorbance was analyzed at 450nm at 0, 24, 48, 72, and 96 hours using an enzyme-linked instrument.

Transwell migration and invasion experiments

Transwell chamber assays were conducted with each experimental condition repeated five times. The suspension containing 1×10^4 glioma cells was added to 24-well Transwell chambers (Corning, USA). The lower chamber was filled with 10% FBS (Gibco, USA) supplemented with 1% penicillin/streptomycin (Beyotime, China). After 24 hours of incubation at 37°C, the migrated glioma cells were fixed with 4% paraformaldehyde and stained with 0.1% crystal violet solution (Beyotime, China). Microscopic images were captured to visualize the migrated cells that passed through the filter. For Transwell invasion assays, the upper chambers were initially coated with Matrigel (BD, USA) and incubated at 37°C for half an hour.

Quantitative real-time PCR

Total RNA in normal brain and GBM tissues were extracted using RNAiso Plus (TaKaRa). The concentration of RNA specimens was measured using a spectrophotometer and then reverse-transcribed into cDNA using the Primescript RT reagent Kit (TaKaRa). Primer sequences for analyzed genes were: ABCA5 forward 5′-GCTTCCAGAACCACCAGACA-3′ and reverse 5′- TCACAACACTGGCAACCCAT-3′, APOBEC3C forward 5′- CAGGC ACAGCAACGTGAATC-3′ and reverse 5′- GGAGCCCCTCCTGGTAACAT-3′, EEPD1 forward 5′- GGGAGGTTCAAGGTGGGAAG-3′ and reverse 5′- TAGGGTCTGTGCAAAGCTCG-3′, HEY1 forward 5′- GGCTGGTACCCAGTGCTTTT-3′ and reverse 5′- GGTCATCTGCAGGATCTCGG-3′, IGFBP2 forward 5′- GCTGGTCATGGGCGAGG-3′ and reverse 5′-CCAGCTCCTTCATACCCGAC-3′, RGS14 forward 5′-CCACCGTGCAAGC TCTGG-3′ and reverse 5′- GGCTGTGGATGCTGAGAGAG-3′, TNFRSF12A: forward 5′-CTCTGAGCCTGACCTTCGTG-3′ and reverse 5′-GTCTC CTCTATGGGGGTGGT-3′, and GAPDH forward 5′-TTCCAGCCTTCC TTCCTGGG-3′ and reverse 5′-TTGCGCTCAGGAGGAGCAAT-3′. Amplification conditions were as follows: 95°C for 20 s, followed by 40 cycles at 95°C for 3 s, and 60°C for 30 s. The relative fold changes in mRNA levels were calculated according to the $2^{-\Delta\Delta CT}$ method.

Immunohistochemistry (ICH)

For IHC, 8 μm sections from formalin-fixed and paraffin-embedded brain tissues were initially subjected to de-waxing and rehydration prior to antigen retrieval. Endogenous peroxidase activity and non-specific antigens were thoroughly blocked using a solution comprising 3% hydrogen peroxide and serum. The subsequent incubation involved exposing the tissue sections to TNFRSF12A, Ki67, MMP9, and MMP2 antibodies overnight at a controlled temperature of 4°C. This step was followed by the application of an anti-rabbit secondary antibody, development using 3,3-diaminobenzidine (DAB) solution, and counterstaining with hematoxylin. Negative controls, meticulously treated with PBS instead of primary antibodies, consistently exhibited no discernible immunoreactivity. To ensure robustness and precision, two independent pathologists meticulously reviewed the stained slides, utilizing a microscope (Olympus, Japan). The comprehensive assessment of TNFRSF12A, Ki67, MMP9, and MMP2 immunohistochemical staining considered both the percentage of positive cells and color intensity. This thorough evaluation provides a reliable basis for the interpretation and understanding of the immunohistochemical results.

QUANTIFICATION AND STATISTICAL ANALYSIS

All statistical analysis and plotting were performed with R software (v4.1.3). Chi-square tests were used for comparisons of categorical variables, and Wilcoxon rank-sum test or T test were used for continuous variables. Pearson's correlation coefficient was used to assess the correlation between two continuous variables. Bonferroni correction was used in the correlation analysis to further ensure the reliability of the results. Kaplan–Meier analyses with a log-rank test applied to compare the outcomes between different subgroups. All p values were two-tailed, and $p < 0.05$ was regarded to be statistically significant. *P < 0.05; **P < 0.01; ***P < 0.001.